



HAL
open science

Understanding the climatic signal in the water stable isotope records from the NEEM shallow firn/ice cores in northwest Greenland

H. C. Steen-Larsen, Valérie Masson-Delmotte, J. Sjolte, S. J. Johnsen, M. Vinther, Francois-Marie Breon, H. B. Clausen, D. Dahl-Jensen, S. Falourd, X. Fettweis, et al.

► To cite this version:

H. C. Steen-Larsen, Valérie Masson-Delmotte, J. Sjolte, S. J. Johnsen, M. Vinther, et al.. Understanding the climatic signal in the water stable isotope records from the NEEM shallow firn/ice cores in northwest Greenland. *Journal of Geophysical Research: Atmospheres*, 2011, 116, 20 pp. 10.1029/2010JD014311 . insu-00647489

HAL Id: insu-00647489

<https://insu.hal.science/insu-00647489>

Submitted on 17 Sep 2020

HAL is a multi-disciplinary open access archive for the deposit and dissemination of scientific research documents, whether they are published or not. The documents may come from teaching and research institutions in France or abroad, or from public or private research centers.

L'archive ouverte pluridisciplinaire **HAL**, est destinée au dépôt et à la diffusion de documents scientifiques de niveau recherche, publiés ou non, émanant des établissements d'enseignement et de recherche français ou étrangers, des laboratoires publics ou privés.

Understanding the climatic signal in the water stable isotope records from the NEEM shallow firn/ice cores in northwest Greenland

H. C. Steen-Larsen,¹ V. Masson-Delmotte,² J. Sjolte,¹ S. J. Johnsen,¹ B. M. Vinther,¹ F.-M. Bréon,² H. B. Clausen,¹ D. Dahl-Jensen,¹ S. Falourd,² X. Fettweis,³ H. Gallée,⁴ J. Jouzel,² M. Kageyama,² H. Lerche,¹ B. Minster,² G. Picard,⁴ H. J. Punge,² C. Risi,^{5,6} D. Salas,⁷ J. Schwander,⁸ K. Steffen,⁵ A. E. Sveinbjörnsdóttir,⁹ A. Svensson,¹ and J. White¹⁰

Received 5 April 2010; revised 17 November 2010; accepted 9 December 2010; published 22 March 2011.

[1] Samples of precipitation and atmospheric water vapor were collected together with shallow firn/ice cores as part of the new deep drilling project in northwest Greenland: the NEEM project. These samples were analyzed for their isotope composition to understand the processes affecting the climatic signal archived in the water stable isotope records from the NEEM deep ice core. The dominant moisture source for the snow deposited at the NEEM-site may be originating as far south as 35°N from the western part of the Atlantic Ocean. The surface atmospheric water vapor appears in isotopic equilibrium with the snow surface indicating a large water exchange between the atmosphere and snowpack. The interannual variability of NEEM shallow firn/ice cores stable isotope data covering the last ~40 years shows an unexpectedly weak NAO signal. Regional to global atmospheric models simulate a dominant summer precipitation in the NEEM area, suggesting that the intermittency of modern winter precipitation is responsible for the lack of a strong NAO imprint. The interannual variability of NEEM isotope data however shows a strong correlation with interannual variations of Baffin Bay sea ice cover, a relationship consistent with air mass trajectories. NEEM deep ice core isotopic records may therefore provide detailed information on past Baffin Bay sea ice extent. NEEM stable water isotope content increasing trend points to a local warming trend of ~3.0°C over the last 40 years.

Citation: Steen-Larsen, H. C., et al. (2011), Understanding the climatic signal in the water stable isotope records from the NEEM shallow firn/ice cores in northwest Greenland, *J. Geophys. Res.*, 116, D06108, doi:10.1029/2010JD014311.

1. Introduction

[2] Polar ice cores offer an extraordinary climate archive. Snow deposited on the Greenland and Antarctic ice sheets captures through its stable isotope composition integrated information about the meteorology [Dansgaard, 1964; Masson-Delmotte et al., 2008]. During the evaporation at the ocean surface and along the air mass trajectory the ratio between the heavy and light water molecules is affected by equilibrium and kinetic fractionation processes [Dansgaard, 1969; Jouzel and Merlivat, 1984; Merlivat and Jouzel, 1979].

[3] Classically, the abundances of HD¹⁶O and H₂¹⁸O of water samples can be measured at high accuracy using mass spectrometers. For the rest of the paper the δ notation will be used, defined as

$$\delta D = \left(\frac{([HD^{16}O]/[H_2^{16}O])_{\text{Sample}}}{([HD^{16}O]/[H_2^{16}O])_{V-SMOW}} - 1 \right) \times 1000$$

$$\delta^{18}O = \left(\frac{([H_2^{18}O]/[H_2^{16}O])_{\text{Sample}}}{([H_2^{18}O]/[H_2^{16}O])_{V-SMOW}} - 1 \right) \times 1000, \quad (1)$$

¹Centre for Ice and Climate, Niels Bohr Institute, University of Copenhagen, Copenhagen, Denmark.

²Laboratoire des Sciences du Climat et de l'Environnement/IPSL, CEA-CNRS-UVSQ, Gif/Yvette, France.

³Inst Climatol, Univ Liege, Liege, Belgium.

⁴Laboratoire de Glaciologie et Géophysique de l'Environnement, Saint Martin d'Hères, France.

⁵Cooperative Institute for Research in Environmental Science, University of Colorado, Boulder, Colorado, USA.

⁶LMD/IPSL, CNRS, UPMC, Paris, France.

⁷Centre National de Recherches Météorologiques/Groupe d'Etude de l'Atmosphère Météorologique, Météo-France, CNRS, Toulouse, France.

⁸Physics Institute, Climate and Environmental Physics, University of Bern, Bern, Switzerland.

⁹Science Institute, University of Reykjavik, Reykjavik, Iceland.

¹⁰Institute of Arctic and Alpine Research, University of Colorado, Boulder, Colorado, USA.

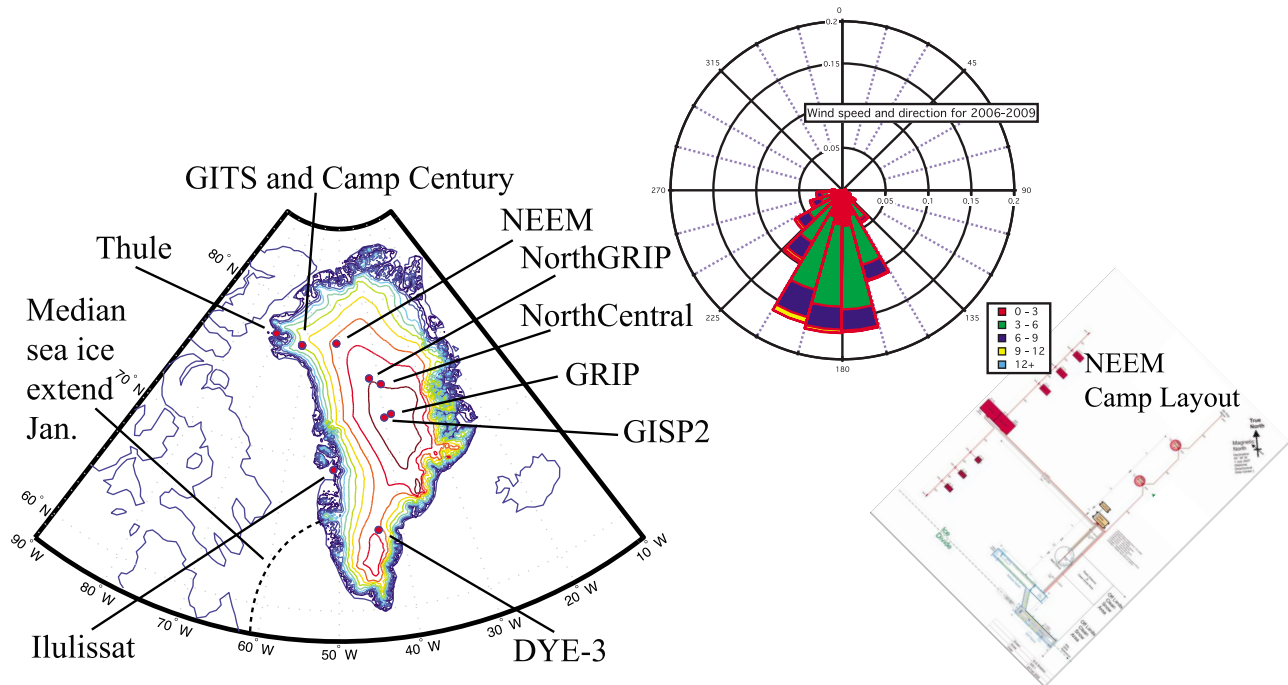


Figure 1. Map of Greenland indicating the position of previous deep ice core drilling sites as well as Greenland Climate Network sites used in this paper. The distribution of wind speed (m/s) and direction is shown together with an outline of the NEEM camp.

expressing the isotopic composition in per mill versus V-SMOW, the Vienna Standard Mean Ocean Water. The combined measurements of $\delta^{18}\text{O}$ and δD on the same water or ice samples give access to the second-order parameter, the deuterium excess (d-excess) defined as the deviation from the global meteoric water line [Dansgaard, 1964]

$$\text{d-excess} = \delta\text{D} - 8 \times \delta^{18}\text{O}. \quad (2)$$

While variations in precipitation $\delta^{18}\text{O}$ and δD are mostly driven by air mass distillation in relationship with the equilibrium fractionation of the moisture during its cooling from the source toward the condensation site, d-excess preserves information about the kinetic fractionation occurring when the moisture initially evaporates from the ocean surface and during snow crystals formation [Dansgaard, 1964; Jouzel and Merlivat, 1984; Merlivat and Jouzel, 1979]. The isotopic signal of the snow is then deposited at the snow surface, recording an integrated meteorological information weighted by precipitation intermittency [Krimmer *et al.*, 1997]. However, postdepositional processes such as wind scouring and ablation add noise into the stable water isotopic record in the snowpack [Fisher *et al.*, 1985]. Moreover, isotopic diffusion linked with the exchange of water vapor between the firn and the surface water vapor, and between the firn and the interstitial vapor, erases the high-frequency snow isotopic composition variability. However, at high-accumulation sites, preservation of seasonal variations in Greenland ice cores is obtained [Vinther *et al.*, 2003]. The remaining isotopic information is then preserved as new snow falls on the firn top, burying the

previous years of snow further down into the ice sheet. This results in a climate archive that can, depending on the annual amount of accumulation, be read year by year [Barlow *et al.*, 1993; Vinther *et al.*, 2003].

[4] Since the 1960s, intensive efforts have been made to extract deep ice cores from the Greenland ice sheet, and investigate the climate variability during the current interglacial, the last glacial period [Dansgaard *et al.*, 1982; Dansgaard *et al.*, 1993], and back into the last glacial inception [North Greenland Ice Core Project Members, 2004]. Stable isotope records from each ice core can also bring specific regional information on moisture origin [Masson-Delmotte *et al.*, 2005], local sea-ice induced changes in atmospheric circulation and mixing [Noone and Simmonds, 2004] or ice sheet topography [Vinther *et al.*, 2009]. The available data have revealed the complexity of the integrated information preserved in Greenland stable isotope composition [Masson-Delmotte *et al.*, 2006] and the need to improve the process-based understanding of its climatic controls.

[5] Within the frame of the International Polar Year, the new deep drilling project – NEEM – was initiated in northwest Greenland in 2007 to obtain a new undisturbed ice core climate record from the last interglacial period, the Eem period (<http://neem.nbi.ku.dk>). The project involves partners from 14 countries and in addition to deep drilling itself also endorses an array of associated programs including meteorological monitoring, firn gas sampling, pit studies, radar surveys and shallow core drillings. The deep drilling site and the NEEM camp are located at 77.45°N and 51.06°W at an elevation of 2484 m above sea level on the

ice ridge going from GRIP through NorthGRIP toward Camp Century (see Figure 1).

[6] To support the interpretation of the stable isotope data to be measured along the main deep core, shallow firn/ice cores were drilled upstream of the camp along the flow line and around the camp as part of the firn gas-pumping program. We report here on high-resolution stable isotope analyses of the upper 40 m of a shallow core drilled in 2007 (NEEM07S3) and the upper 15 m of a shallow core drilled in 2008 (NEEM08S3A), spanning the periods 1964–2005 and 1978–2007, respectively.

[7] To support the interpretation of the stable water isotope content found in the firn/ice cores an associated surface isotope program was carried out in 2008 in parallel with the set up of the camp and drilling facilities. Here, we report on the monitoring of the precipitation and water vapor isotopic composition during this 2008 field season. The measurements of the δD and $\delta^{18}\text{O}$ composition of these samples provide further understanding of the meteorological controls on daily precipitation isotopic composition at the NEEM site.

[8] In the recent two decades a suite of global and regional GCM with isotope modules have been developed to improve the understanding of the interaction between isotopes in precipitation and the climate [Hoffmann *et al.*, 1998; Lee *et al.*, 2007; Mathieu *et al.*, 2002; Noone and Simmonds, 2002; Risi *et al.*, 2010a; Sturm *et al.*, 2005]. The global and regional GCMs supplemented single source distillation models [Ciais and Jouzel, 1994; Johnsen *et al.*, 1989] by most importantly including mixing of the vapor from several sources. Mixing of vapor from several sources was initially studied by Fisher and Alt [1985] and Fisher [1990]. From early and more current studies it is evident that the isotopic composition of precipitation in Antarctic and Arctic is strongly dependent on the supersaturation during formation of snow crystals and the temperature at which snow crystals begin to form in the cloud [Fisher, 1991; Jouzel and Merlivat, 1984; Schmidt *et al.*, 2005]. In this paper we will use collected precipitation samples to study the supersaturation using a distillation model and compare interannual and annual variability in modeled isotope values at NEEM from a regional and global GCM with the interannual and annual variability observed in a shallow core.

[9] In this paper, the new NEEM data are first presented, from meteorological data to precipitation, water vapor, and shallow firn core isotopic data. In section 4.1, isotopic Rayleigh model experiments are used to characterize the NEEM moisture source characteristics and to understand the origin of surface water vapor. A statistical correlation analysis is performed to quantify the local and large-scale climatic controls on the interannual variability of the NEEM water stable isotope records. Regional and global atmospheric circulation model outputs are investigated to explore the specificities of modern climate in the NEEM Greenland sector, and to assess the ability of atmospheric models to depict the local climate and water stable isotope composition.

[10] In the line of the work of Grootes and Stuiver [1997], this paper therefore aims to integrate data from shallow cores, precipitation and water vapor measurements with models to obtain a better understanding of the processes generating the climatic signal found in the ice core. This will

form the basis for the interpretation of the climatic signal deeper in the ice sheet.

2. Data Description

2.1. NEEM Meteorological Characteristics From Remote and Site-Based Observations

[11] During the period from 2006 to 2009 an automatic weather station has been logging meteorological conditions (air temperature and relative humidity using Campbell Sci. HMP45C, ± 0.1 K and $\pm 5\% < 90\% \text{RH}$ and $\pm 10\% > 90\% \text{RH}$, wind direction and speed using RM Young propeller-type vane, $\pm 5^\circ$ and $\pm 0.1 \text{ ms}^{-1}$, and station pressure using Vaisala PTB101B, ± 0.1 mb) for the NEEM site as part of the Greenland Climate Network [Steffen *et al.*, 1996; Steffen and Box, 2001]. However, due to some faulty batteries, the power dropped during the winter and data could only be recorded from May to October. These monthly mean values are shown in Figure 2c together with the monthly mean values for the NorthGRIP and GITS station (positions indicated on Figure 1).

[12] From temperature measurements of the shallow holes drilled at NEEM (J. Schwander, personal communication, 2009), we know that the annual mean temperature is $\sim -29^\circ\text{C}$. We combine this annual mean temperature estimate with the meteorological data to estimate the temperature at NEEM for the months November to April under the assumption that the shape of the temperature profile is the same as for NorthGRIP. The estimated seasonal temperature cycle is shown in Figure 2c. The automatic weather station also recorded the wind direction and wind speed as shown in Figure 1. The majority of wind directions were found to come from the south with a wind speed between 3 and 6 ms^{-1} . Due to the lack of snow gauge instruments, we have no direct quantitative information on the precipitation amount and intermittency. However, using LIDAR profiles collected by the CALIPSO satellite, we can estimate the seasonal distribution of days with presence of low clouds for the different seasons [Vaughan *et al.*, 2009] based on a visual inspection of the backscattering profiles. By making the assumption that low clouds may be indicative of precipitation at NEEM, which is supported by in situ observations during the summer season, we can estimate the seasonal distribution of days with precipitation. By analyzing the LIDAR profiles passing through a 100 km by 100 km footprint centered around the NEEM site we find for 2008 that 40%, 45%, 55%, and 28% of the profiles during the spring, summer, fall, and winter, respectively, show indications of precipitation. This does however not give any information about the amount of precipitation. For the majority of days with precipitation around NEEM, the elevation of the clouds is about 0.5 to 1 km height above the snow surface. This satellite information suggests more scarce precipitation events during winter than during the rest of the year, at least for 2008.

[13] Satellite microwave data from SMMR and SSM/I radiometers have almost continuously measured brightness temperatures in the microwave domain since 1979 over the polar regions, with a spatial resolution of 10–60 km. Before August 1987, data is available every second day at NEEM, while daily microwave data are available after 1987. The presence of liquid water at the surface can be detected from microwave data. The classical algorithm used to detect

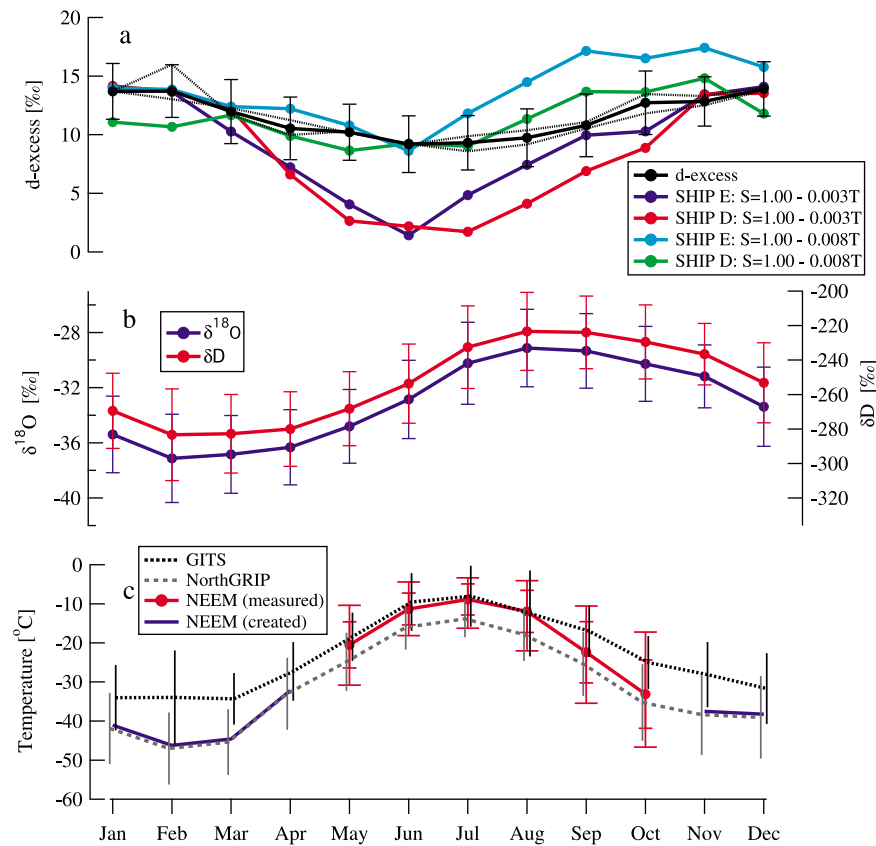


Figure 2. (a) The modeled and observed annual d-excess cycle. The observed d-excess cycle from the NEEM07S3 record is shown by the black solid line. Error bars indicate the 1σ of the estimated monthly values. Dividing the NEEM07S3 record into two parts covering about the first and the last 20 years, respectively, reveals the two thin black dashed lines. Using the distillation model of *Johnsen et al.* [1989] and moisture origin from SHIP E and D, respectively, and with different supersaturation functions gives the annual d-excess cycle (solid dark blue, red, light blue, and green lines, respectively). (b) The annual $\delta^{18}\text{O}$ and δD cycle estimated from the NEEM07S3 record (blue and red solid lines). Error bars indicate the 1σ of the estimated monthly values. (c) The annual ice sheet temperature cycle from the Greenland Climate Network at GITS and NorthGRIP (dotted and dashed black lines). Error bars indicate the 1σ of temperatures for each month. Estimated for the period 1997–2007 and 1997–2002, respectively. The measured temperature at NEEM is shown by the solid red line. Error bars indicate the 1σ and 5%–95% quartile of the temperature for the specific months. Blue solid line indicates the estimated monthly temperature during the winter season at NEEM.

Greenland melt [*Abdalati and Steffen, 2001*] does not detect any melt event at NEEM. However, using brightness temperature at 19 GHz and horizontal polarization with a methodology developed originally for the Antarctic [*Picard et al., 2007; Torinesi et al., 2003*], melt events can be detected at NEEM on specific days. Only 6 melt events are detected at NEEM, on 26-06-2007, 24-07-2005 and 26-07-2005, 04-08-2001, 17-07-1999 and 18-07-1999, and 14-07-1995. No events are detected prior to 1995 (however having the sampling bias prior to 1987 in mind). Interestingly, slightly closer to the coast (79.09°N, 57.08°W), all the melt events detected at NEEM site are also recorded, albeit with a longer duration (several days), and four additional events are detected (09-08-2008, 29-06-2002, 20-07-2002 and 25-07-2002, and 25-07-1979). Closer to the coast, melt events are detected each summer since 1993 but prior to 1993 melt is only detected during the summer of 1979.

2.2. Precipitation

[14] Twenty-five precipitation samples were collected at NEEM from 07/07/08 to 08/14/08. During the sampling campaign four major precipitation events occurred and are numbered 1 to 4. Events 1, 2, and 4 are characterized by an increased depletion accompanied by a d-excess increase; opposite isotopic trends are observed for event 3. Common for the precipitation events are the very high relative humidity (RH), which is close to 100% saturation, and the relative high 2 m temperatures between -10 and -5°C . During precipitation events no diurnal cycle in neither the RH nor temperature is observed and the surface wind was observed to come from the west.

[15] During the full sampling campaign, four samples with unusual low d-excess close to zero were collected and are highlighted by circles in Figure 3. The δD - $\delta^{18}\text{O}$ of the precipitation samples are shown in Figure 4 using blue

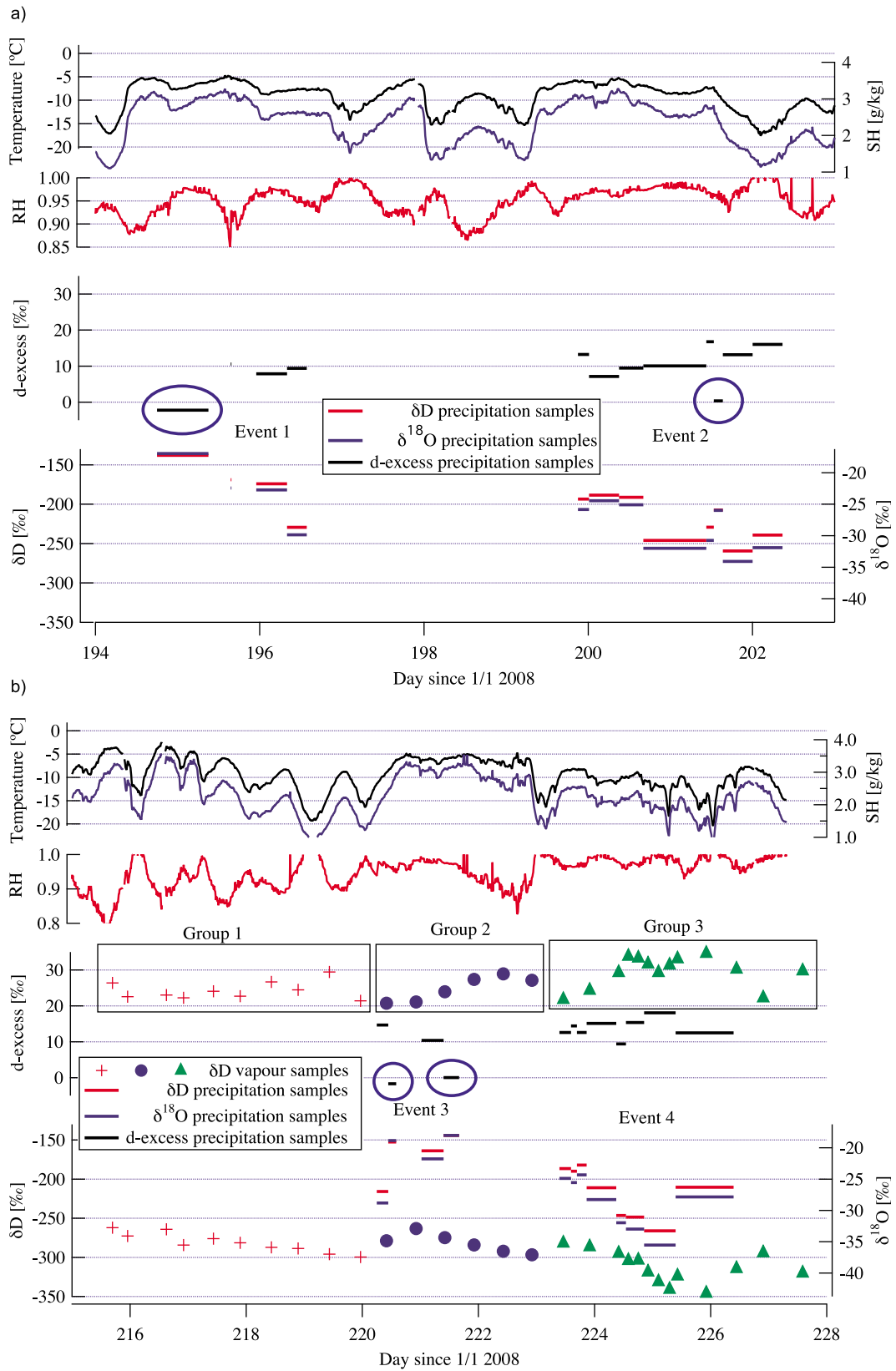


Figure 3

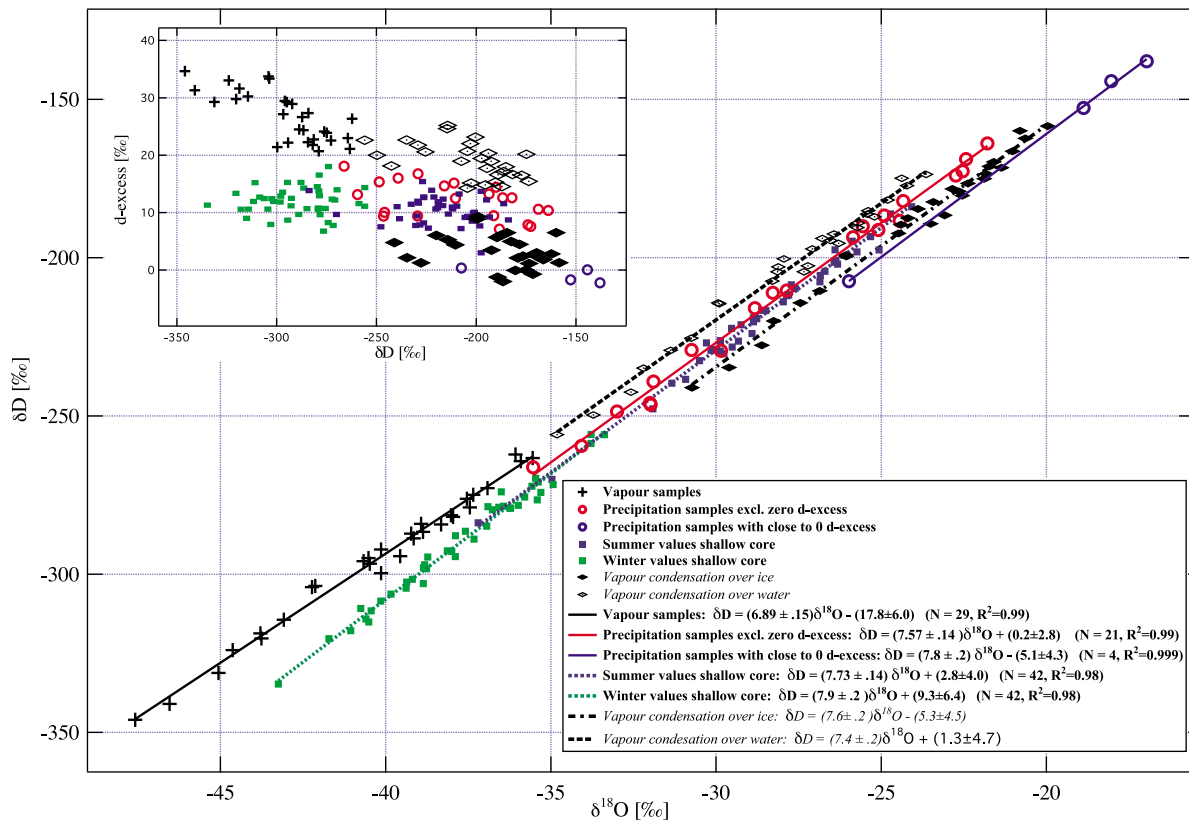


Figure 4. The δD - $\delta^{18}O$ of the atmospheric water vapor samples (black crosses), the precipitation samples (red and blue circles for sets without or with close to zero d-excess samples, respectively), summer season maximum values of the NEEM07S3 record (black square), winter season minimum values of the NEEM07S3 record (green square), and the condensate (over ice and over water) in isotopic equilibrium with the water vapor (filled and open diamonds). Lines indicate best linear fit to the different samples. Modeled parameters are indicated by italic while measurements are indicated in bold. The insert shows d-excess- δD of the same data points as shown in the main figure.

circles for the samples, which show very low d-excess value (Set A), and red circles for the rest of the samples (Set B). δD and $\delta^{18}O$ data from Set B show a strong linear correlation, an observed local meteoric water line given $\delta D = (7.6 \pm 0.10)\delta^{18}O + (0.2 \pm 2.8)$, where the uncertainty refers to 1 standard deviation and $R^2 = 0.99$.

2.3. Atmospheric Water Vapor

[16] During the period from 08/03/08 to 08/15/08, surface atmosphere water vapor was collected using a cryogenic vapor trap [Craig and Gordon, 1965]. Atmospheric water vapor was collected twice a day, in the morning and in the evening, except on August 12th–13th where sampling was

performed every 4 h. The collected water vapor $\delta^{18}O$ values varied from approximately -35‰ to -48‰ while the δD values varied between -260‰ to -346‰ . Within 24 h we observed changes in $\delta^{18}O$ and δD as large as about 6‰ and 46‰, respectively. The water vapor samples can be combined into three groups, coherently with the precipitation events (Figure 3). Since we observed precipitation at NEEM on July 30th, August 8th to 9th, and again on August 11th to 14th we divide the vapor samples into periods ranging from August 3rd to 7th, August 8th to 10th, and August 11th to 15th. Within each vapor group, the water vapor isotopic composition exhibits a strong correlation with the surface air specific humidity (SH) ($R^2 = 0.86, 0.45, \text{ and } 0.81$ for group

Figure 3. Precipitation samples are indicated by horizontal solid lines indicating the time and duration of sampling. Red, blue, and black lines are used for δD , $\delta^{18}O$, and d-excess, respectively. The numbers indicate the different events. Blue circles indicate samples with very low d-excess value. The 2 m temperature, specific humidity, and relative humidity are shown by the black, blue, and red solid lines, respectively. Atmospheric water vapor samples (red crosses, blue dots, and green triangles, respectively) are separated into different groups as indicated by the boxes. Only the δD and d-excess is shown for the vapor samples. The maximum and minimum values for $\delta^{18}O$, δD , and d-excess of the precipitation samples are -16.97‰ , -137.95‰ , and -2.2‰ and -35.54‰ , -266.20‰ , and 18.1‰ , respectively. For events 1, 2, 3, and 4 we observe large amplitudes of δD changes during the course of the snowfall events (-92‰ , -71‰ , $+72\text{‰}$, and -79‰).

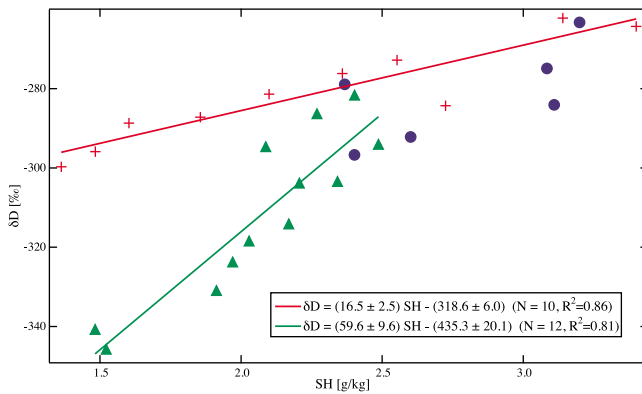


Figure 5. The δD composition of the water vapor samples versus the specific humidity at time of sampling. The samples are divided into the same groups as indicated by the boxes in Figure 3. The best linear fits to group 1 and group 3 are displayed.

1, 2, and 3; see Figure 5). Such a linear relationship was also reported by *White and Gedzelman* [1984] for vapor collected from the atmosphere near Palisade, New York, United States, whereas *Wen et al.* [2010] found the isotopic composition of the atmospheric vapor over Beijing, China, on nonraining days to vary linearly with the logarithm of the mixing ratio. For the groups spanning the periods August 3rd to 7th, and August 11th to 15th, which show the highest linear correlation, the relationship between specific humidity and δD is given by $\delta D = (16.5 \text{ SH} \pm 2.5) \text{ (g/kg)} - (318.6 \pm 6.0)$ ($R^2 = 0.86$, $N = 10$) and $\delta D = (59.6 \pm 9.6) \text{ SH (g/kg)} - (435.3 \pm 20.1)$ ($R^2 = 0.81$, $N = 12$). These relationships reflect increased isotopic depletion of the driest air parcels.

[17] The isotopic values of the complete set of water vapor samples are shown in a δD - $\delta^{18}O$ diagram in Figure 4. The relationship between δD and $\delta^{18}O$ is found to be $\delta D = (6.89 \pm 0.15) \delta^{18}O - (17.7 \pm 6.0)$ ($R^2 = 0.99$). The high degree of linearity found for the δD - $\delta^{18}O$ relationship of our water vapor samples demonstrates the quality of our sampling. Section 4.3 will combine isotopic modeling with the NEEM observed precipitation and water vapor δD - $\delta^{18}O$ slopes to discuss the origin of surface moisture.

2.4. Shallow Firn/Ice Cores Dating and Measurements

[18] We describe hereafter the dating and the results from 2.5 and 5.0 cm isotopic measurements conducted on the shallow cores drilled in 2007 and 2008 (NEEM07S3 and NEEM08S3A) (Table 1).

[19] Density measurements were performed on NEEM07S3 in the cold-room laboratory in Copenhagen while the NEEM08S3A core was processed in the field (Figure 6). The depth density profiles are well explained by the densification model of *Herron and Langway* [1980] using a critical density of 550 kg/m^3 , an initial density of 340 kg/m^3 , and the climatology of the NEEM site. The absolute dating of the shallow ice cores is based on counting annual layers in the isotopic records; it is verified using volcanic horizons detected from electrical conductivity measurements conducted in the cold-room laboratory in Copenhagen and in the NEEM science trench [*Hammer*, 1980]. The accuracy of the dating is higher than 1 year. From the annual layer thickness and the density record, the annual accumulation rate is obtained (Figure 7c). On average, the NEEM accumulation rate is estimated to be 22 cm ice equivalent.

3. The Nature of the Shallow Firn/Ice Core Records

3.1. Back-Diffused Shallow Ice Core Data

[20] The loss of seasonal isotopic amplitude with depth is caused by molecular diffusion in the firn pore space [*Johnsen*, 1977; *Johnsen et al.*, 2000]. It is therefore necessary to reconstruct the original isotopic seasonal amplitude to quantify past interannual climate variability. The measured and back-diffused reconstructed profiles are shown in Figure 7g, and panel a shows the ratio between the back-diffused yearly amplitude and the amplitude of the original data. After ~ 10 years the seasonal amplitude is damped to $\sim 50\%$ of the original signal, a feature which is correctly captured by the theoretical diffusion length calculation [*Johnsen et al.*, 2000] (Figure 7a). Another result of the diffusion is the phase shift of the d-excess, which forces it to be in phase with $\delta^{18}O$ and δD after some years depending on the diffusion length. It is therefore important in order to discuss the d-excess annual cycle that the isotopic profiles of $\delta^{18}O$ and δD are back-diffused. Since the diffusion is not affecting the annual isotopic profile of any significant amount it is possible to compare the annual isotopic record of the NEEM07S3 core with the NEEM08S3A core isotopic record. This is done in section 3.2 with regard to signal-to-noise ratio. Since δD is not available for the NEEM08S3A core it is not possible to properly back diffuse this record. This means that no signal-to-noise ratio can be studied on the summer and winter values. The mean annual $\delta^{18}O$ level is $-33.0 \pm 1.6\%$ and the average annual d-excess value is $11.5 \pm 1.0\%$.

[21] Figure 7b shows the interannual variations of the raw and back-diffused data, and the annual, DJF and JJA

Table 1. Summary of the Two Shallow Firn/Ice Cores (NEEM07S3 and NEEM08S3A) Used in the Paper^a

Name	Year Drilled	Depth	Sampling Resolution	Status of $\delta^{18}O$ and δD Measurements	$\delta^{18}O$ and δD Uncertainty	Dating Method	Dated Period
NEEM 07S3	2007	80.05 m	5 cm from 1.15 to 12.10 m 2.5 cm from 12.10–80.05 m	$\delta^{18}O$ on 1.15–80.05 m δD on 1.15–19.65 m	$\delta^{18}O$ (CIC): 0.08% δD (LSCE): 0.5%	Annual layer counting down to 19.65 m	1964–2005
NEEM08S3A	2008	13.15 m	2.5 cm from 0.0–13.15 m	$\delta^{18}O$ on 0.0–13.15 m No δD	$\delta^{18}O$ (LSCE): 0.05%	Annual layer counting down to 13.15 m	1978–2007

^aOnly data down to 19.65 m of the NEEM07S3 core is presented in the paper due to lack of δD measurements on the rest of the core.

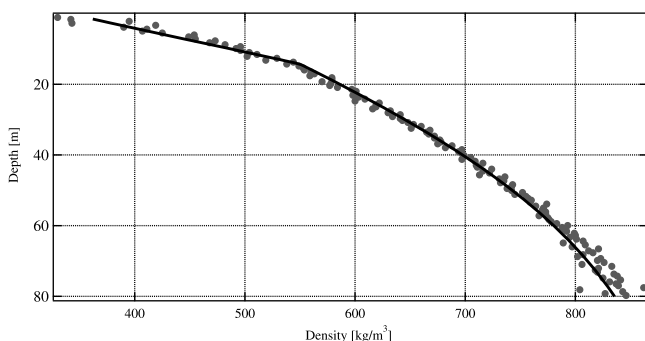


Figure 6. The bag-density measurements of the NEEM07S3 core (55 cm sample) together with the best fit of a Herron-Langway density model using the model parameters for the initial density (340 kg/m^3), the critical density (550 kg/m^3), and the climatology of the NEEM site.

variations of $\delta^{18}\text{O}$ and d-excess are displayed on Figures 8d and 8e. A linear fit to the mean annual $\delta^{18}\text{O}$ values reveals an increasing trend over the last 40 years of $2 \pm 0.8\text{‰}$. The trend seen in the summer and winter values are not significantly different from the trend in the mean annual value. Using the spatial relationship between temperature and $\delta^{18}\text{O}$ value of 0.67‰/K , supported by the temporal relationship between GRIP borehole temperature and $\delta^{18}\text{O}$ data [Johnsen *et al.*, 1999], this $\delta^{18}\text{O}$ increasing trend translates into a warming trend to first order of $\sim 3.0 \pm 1.2^\circ\text{C}$ over the past 40 years as comparison no significant trend is seen in the mean annual coastal temperatures from Ilulissat over the last 40 years. However, the Ilulissat temperatures have over the last 10 years increased with $\sim 2.2 \pm 1.6^\circ\text{C}$.

[22] Using the back-diffused isotopic record, the 40 year records of $\delta^{18}\text{O}$, δD and d-excess seasonal variations can be stacked to characterize the mean annual cycles (Figures 2a and 2b). By construction, the dating produces annual $\delta^{18}\text{O}$ cycles with respective minima and maxima in the first of February and first of August. From back-diffused data, the mean NEEM seasonal $\delta^{18}\text{O}$ amplitude is estimated to $\sim 4.4\text{‰}$ (Figure 2). Comparing this value to the compiled values by Fisher *et al.* [1985] reveal that it is below the 95% confidence limit of the distribution of previous observations in Greenland. The raw d-excess seasonal cycles exhibit a 3 month lag [Johnsen *et al.*, 1989], but the phase lag between $\delta^{18}\text{O}$ and d-excess is affected by diffusion. The back-diffused deuterium excess is minimum around Jun–Jul and maximum in Dec–Jan–Feb, therefore showing a ~ 4 – 5 month lag with respect to $\delta^{18}\text{O}$ and closer to being in antiphase. The average minimum and maximum value of the d-excess annual cycles is ~ 9 and $\sim 14\text{‰}$, respectively. With an average at $\sim 11.5\text{‰}$ which is quite high compared to an average d-excess level at GRIP and NorthGRIP of $\sim 9.5\text{‰}$ and 10.5‰ , respectively (Table 2).

3.2. Signal-to-Noise Ratio

[23] Because of overlap between NEEM07S3 and NEEM08S3A from 1979 to 2005, it is possible to characterize the signal-to-noise ratio (SNR) of the annual $\delta^{18}\text{O}$ and annual accumulation records. Using the terminology of Fisher *et al.* [1985] on SNR analysis of the $\delta^{18}\text{O}$ record for

the 2 ice cores reveals the variance of the signal and of the noise to be 2.5‰^2 and 0.9‰^2 , respectively. Similarly, for the annual accumulation the variance on the signal and on the noise is found to be $1.4 \times 10^{-3} \text{ m}^2$ and $1.0 \times 10^{-3} \text{ m}^2$. As a result, the SNR for the annual $\delta^{18}\text{O}$ record and annual accumulation record are found to be 2.7 and 1.6, respectively, comparable to previous studies conducted for the north central site and Camp Century [Fisher *et al.*, 1985], which is comparable to NEEM in terms of mean annual temperature and latitude, respectively. However, the north central site has a significant lower annual accumulation, which explains the lower SNR for the accumulation compared to NEEM, while Camp Century has significantly more annual accumulation leading to a higher SNR. The maximum value of the height of the sastrugies (assuming them to have a sine curve shape) can be estimated from the noise on the accumulation records [Fisher *et al.*, 1985] at $\sim 0.1 \text{ m}$, which is in good agreement with in situ observations of surface undulations.

4. Analysis of the Precipitation and Water Vapor Samples

[24] In section 2.2 the presented Set B precipitation samples show a strong linear correlation. This suggests a common moisture source for all of the Set B precipitation samples, and a different moisture origin for Set A with a very different δD – $\delta^{18}\text{O}$ relationship. Very low d-excess values can also be generated in the case of reevaporation of snow crystals during precipitation. However, the meteorological data do not depict low relative humidity above the snow surface during these A events; but the conditions above the snow surface are not necessarily coupled with the conditions higher up in the atmosphere. Another explanation for low-precipitation d-excess data lies in moisture source characteristics. Low kinetic effects are expected if evaporation occurs over a cool ocean surface with high surface air RH; these characteristics can be found at high latitudes. Back-trajectories have been calculated using the HYSPLIT–Hybrid Single Particle Lagrangian Integrated Trajectory Model from Air Resources Laboratory, NOAA [Draxler and Rolph, 2003] and NCEP’s Global Data Assimilation System 1-degree latitude-longitude resolution for each NEEM 2008 precipitation event. For all events of set B, the air mass trajectory is originating from the southwest of NEEM, while all events of set A coincide with an Arctic northward air mass origin (not shown).

4.1. Using Isotopic Rayleigh Modeling to Determine Moisture Origins

[25] In the following, we focus on the precipitation samples with “normal” d-excess (Set B) expected to have a common moisture source. We first explore the parameters of a Rayleigh distillation model [Johnsen *et al.*, 1989], which are compatible with the NEEM data.

[26] The distillation model takes into account the kinetic isotope fractionation effects during evaporation [Merlivat and Jouzel, 1979] and formation of snow [Jouzel and Merlivat, 1984], using the supersaturation function relating temperature and humidity over the surface of the snow crystals during formation [Hoffmann *et al.*, 1998; Masson-Delmotte *et al.*, 2005]. The model results, and particularly

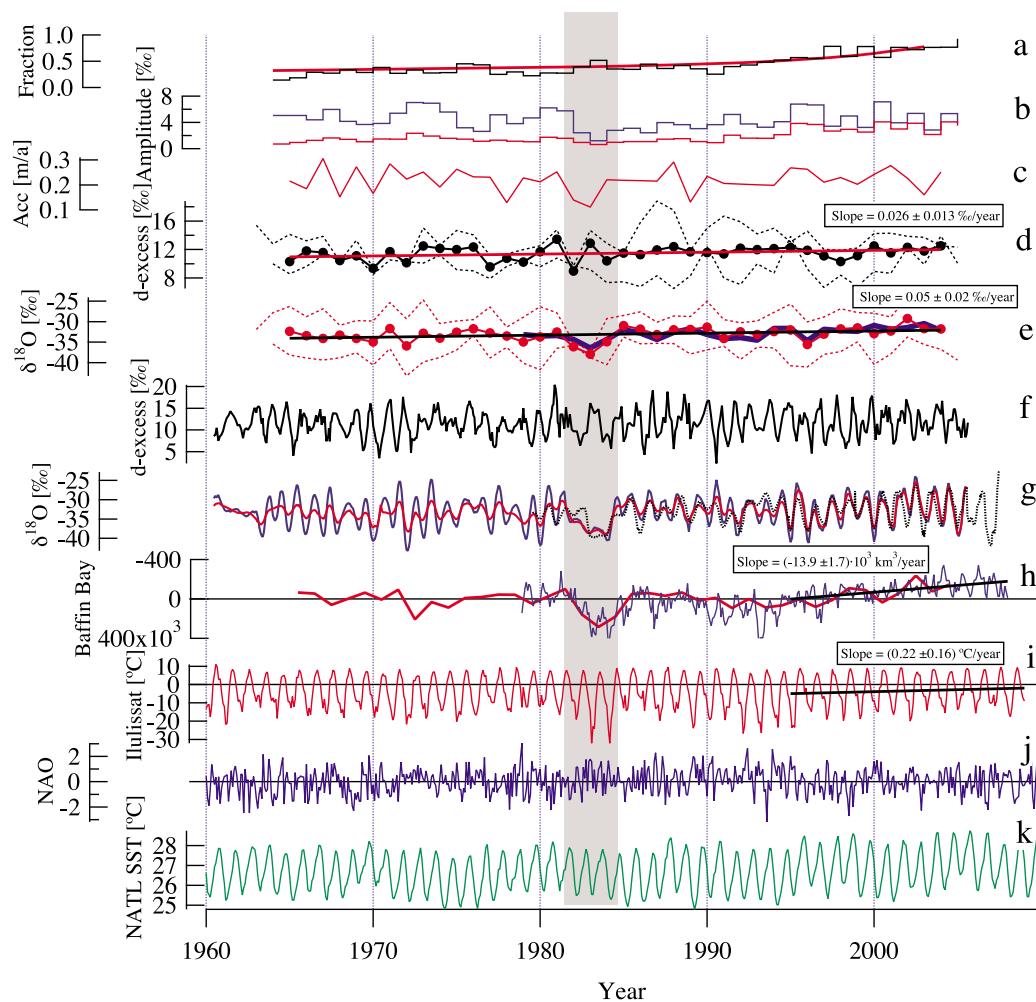


Figure 7. (a) The ratio between the annual back-diffused isotopic amplitude and the observed annual amplitude shown together with the theoretical prediction. (b) Back-diffused annual amplitude (blue solid line) together with the observed annual amplitude (red solid line). (c) Annual accumulation in ice equivalents. (d) Mean annual d-excess (black solid line) together with JJA and DJF values (upper and lower black dashed lines). The best linear fit to the mean annual d-excess values shows an increasing slope of $\sim 0.026\%/yr$ (solid red line). (e) Mean annual $\delta^{18}O$ (red solid line) together with JJA and DJF values (upper and lower dashed red lines). The best linear fit to the mean annual $\delta^{18}O$ values shows an increasing slope of $0.05\%/yr$ (solid black line). The best fit with a multivariable linear regression using Baffin Bay Annual Sea Ice Anomaly, Ilulissat annual temperature, NAO winter anomaly, and NATL winter anomaly (solid blue line). (f) The d-excess after back-diffusing the measured signal. (g) The measured $\delta^{18}O$ profile from NEEM07S3 (red solid line) shown together with the back-diffused $\delta^{18}O$ profile (blue solid line). For comparison the measured $\delta^{18}O$ profile from NEEM08S3A is shown (black dash line). (h) The Baffin Bay Sea Ice extent from satellite observation (blue solid line). Notice reversed axis. The estimated Baffin Bay Sea Ice extent based on a multivariable linear regression of NEEM07S3 annual $\delta^{18}O$, Ilulissat annual temperature, NAO winter anomaly, and NATL winter anomaly. The sea ice extent shows a decrease of $\sim 14 \times 10^3 \text{ km}^3/yr$ since 1995 to present (solid black line). (i) The observed temperature record from Ilulissat (69.2°N 51.1°W). The temperature shows an increase of $\sim 0.2^\circ\text{C}/yr$ since 1995 to present (solid black line). (j) Observed NAO index. (k) The sea surface temperature of the North Atlantic Ocean in the region $5\text{--}20^\circ\text{N}$ and $30\text{--}60^\circ\text{W}$. The gray vertical bar indicates the very strong anomaly in the BBASIA also seen in the NEEM isotopes.

the simulated d-excess are very sensitive to the model parameterizations. In this article, we have not modified the threshold for ice crystal formation [Fisher, 1991] but have instead adjusted the supersaturation function.

[27] The model can be used in a direct way by prescribing the initial conditions (moisture source sea surface tempera-

ture SST and relative humidity RH at 10 m above the ocean surface) and the Greenland snow $\delta^{18}O$: the model iterates the path from the source region to the sink region until the prescribed final $\delta^{18}O$ value is obtained. From this best fit path, the model also simulates δD and d-excess. Here we use this model in an inverse mode by prescribing NEEM

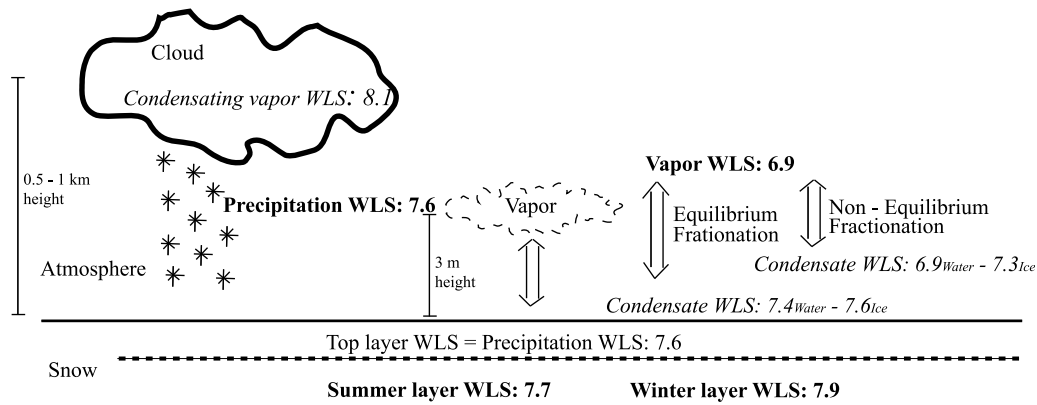


Figure 8. The key factors in the local hydrological cycle above the snow surface. The numbers indicate the meteoric water line slope (WLS) of δD - $\delta^{18}O$, which we use to determine from where the sampled water vapor originates. Vapor is collected at 3 m height. CALIPSO data indicate that the clouds bringing in precipitation are about 0.5 and 1 km above the snow surface. We use italic to illustrate slopes we obtain from models and bold to illustrate slopes we obtain from direct measurements of samples.

$\delta^{18}O$ and δD to estimate the moisture source SST and RH. By optimizing the simulated NEEM ($\delta^{18}O$, δD) slope, we obtain $RH \sim 0.60 \pm 0.05$ and $SST \sim 20 \pm 4^\circ C$ using the commonly used value for the supersaturation function, $S = 1.00 - 0.003T$. Outputs (not shown here) of RH from global circulation models such as CCM3.6.6 forced by present-day SST fields indicating that such a set of parameters are not to be found in the Atlantic Ocean for July and August during which the precipitation samples were collected at NEEM.

[28] Since the current model set up is not able to simulate a realistic source condition we used a fixed SST and RH of the source region while tuning the supersaturation function to simulate the observed relationship between δD and $\delta^{18}O$ found in the precipitation samples from NEEM. *Johnsen et al.* [1989] and *Trigo* [2006] showed that the western part of the North Atlantic between $30^\circ N$ and $50^\circ N$ is a major center for the formation of cyclonic systems in the North Atlantic. We therefore assume that this area is the most likely source region, with $\sim 23^\circ C$ SST and ~ 0.8 RH. With this strong hypothesis on a single moisture source, the model can only capture the NEEM summer precipitation (δD - $\delta^{18}O$) slope of 7.6 if the supersaturation function is given by $S = 1.00 - 0.008T$. Using the uncertainty estimations of the linear regression of δD - $\delta^{18}O$, we find that the supersaturation function previously used, $S = 1.00 - 0.003T$, is outside the estimated ± 1 standard deviation of the new supersaturation function.

[29] This estimated temperature dependence of the supersaturation function is higher than previous reported

values. Using simple distillations models, *Petit et al.* [1991] reported temperature slopes varying from -0.0025 to -0.0038 in order to reasonable fit the Antarctic data. Using data from the same region, *Fisher* [1991] obtained values from -0.003 to -0.009 . With atmospheric general circulation models, recent studies have also reported different supersaturation adjustments than the classical temperature dependence of -0.003 [*Hoffmann et al.*, 1998]. In order to capture $\delta^{17}O$ in Vostok precipitation, *Risi et al.* [2010b] used a low value of -0.002 , while other studies used higher slopes such as -0.004 to capture Antarctic d-excess data [*Schmidt et al.*, 2005] or the isotopic signature of ENSO [*Tindall et al.*, 2009] (albeit without d-excess constraints).

[30] We note that our study based on precipitation samples differs from previous works, which relied on surface snow data to adjust the supersaturation function. Surface snow samples integrate precipitation events over weeks to years in Greenland or Antarctica. During this period, post depositional processes might have altered the isotopic composition and therefore the d-excess levels. Here, we use direct sampled precipitation, which have most of the time only been averaged for about 3–6 h and should therefore have undergone minimum post depositional processes. Simulations conducted with atmospheric general circulation models have shown that Rayleigh distillation models best perform on short time scales [*Noone and Simmonds*, 2002].

[31] Our results explicitly assume a single moisture source, which is likely unrealistic. *Fisher* [1990] showed using a zonally averaged simple distillation model that 70%

Table 2. Summary of Other Deep Ice Core Drilling Sites in Greenland: Position And Elevation, Their Isotopic Composition, and Climatology

	NEEM	GRIP	NorthGRIP	Dye-3	Camp Century
Position	77.45°N 51.06°W	72.58°N 38.50°W	75.10°N 42.32°W	65.18°N 43.83°W	77.18°N 61.15°W
Elevation	2484 m	3230 m	2919 m	2490 m	1890 m
Mean temperature	$-29^\circ C$	$-32^\circ C$	$-32^\circ C$	$-20^\circ C$	$-24^\circ C$
Mean $\delta^{18}O$	-33‰	-35.2‰	-35.5‰	-28‰	-29‰
Mean d-excess	11.5‰	9.5‰	10.5‰	8.3‰	NN
Accumulation Water equivalent	20 cm/a	23 cm/a	19 cm/a	50 cm/a	35 cm/a

of the accumulation at Crête, Greenland, originates from the Atlantic Ocean between 20°N and 55°N. Despite contributions from various latitudes, their accumulation weighted source latitude appears to be ~35°N, which is in very good agreement with our working hypothesis. *Werner et al.* [2001] used a GCM to depict that origin of precipitation at Summit, Greenland, consist of 28% moisture from the northern Atlantic and 14% from the tropical Atlantic. The d-excess from these two regions was simulated to be ~4‰ and 11‰, respectively, and to control the seasonal d-excess in the snow at Summit.

[32] We are finally aware that the results from the distillation model are affected by the closure assumption, which neglects advection and mixing of vapor above the main moisture source. *Armengaud et al.* [1998] have indeed demonstrated differences in the simulated Greenland d-excess when using the closure assumption and when using prescribed vapor fields from GCMs. We have therefore prescribed the isotopic composition of the initial vapor with isotopic values obtained from ECHAMiso calculated vapor fields (which account for mixing). We have repeated the same procedure to estimate the supersaturation function that best captures the observed relationship between δD and $\delta^{18}O$ in NEEM precipitation samples. In this case, the best fit is obtained when assuming that the majority of the vapor originates 10° further south (from Weather ships D (44°N, 41°W) and E (35°N, 48°W) [*IAEA/WMO*, 1969–1979]), than what was found when assuming closure assumption. In this case, the supersaturation is optimized to $S = 1.00 - 0.007T$. Using this new supersaturation function and the isotopic vapor fields from ECHAMiso does not improve the fit with the NEEM d-excess seasonal cycle (discussed in section 4.2). By assuming vapor from around SHIP A at 62°N 33°W (using both closure assumption and ECHAMiso vapor fields) returns a temperature dependence of the supersaturation smaller than -0.01 in order to simulate the precipitation samples. This sensitivity test to the initial vapor isotopic composition (either using the closure assumption or the ECHAM fields) supports the use of a single source situated between 30°N and 50°N for the precipitation samples collected at NEEM.

4.2. Modeling the d-Excess Seasonal Cycle

[33] Based on the mean seasonal cycle of the back-diffused shallow firn/ice core data (Figure 2b), the mean $\delta^{18}O$ cycle is used as an input in the distillation model [*Johnsen et al.*, 1989]. Using the new supersaturation function, the annual NEEM precipitation d-excess cycle is calculated using different source regions defined by SHIP D and SHIP E. The modeled d-excess with the new and the old supersaturation functions are compared to the d-excess of the stacked shallow firn core data (Figure 2a). With the new supersaturation function (only adjusted to capture the NEEM δD - $\delta^{18}O$ slope), the model is able to capture reasonably well the amplitude and timing of the d-excess cycle. Assuming a southward moisture source shift from Ship D to Ship E during late fall, and back to Ship D in March would bring the model results even closer to the NEEM seasonal d-excess cycle, suggesting seasonal changes in NEEM moisture origin. This “best guess” model tuning and moisture source compatible with NEEM data is used for calculations of water vapor isotopic composition in section 4.3.

4.3. Origin of the Water Vapor Above the Snow Surface

[34] We explore here the isotopic constraints available to assess the origin of the surface vapor that we have sampled at NEEM. First, we assess the hypothesis that the surface vapor is directly linked with the atmospheric moisture providing NEEM precipitation. We then analyze the hypothesis that the local surface snow is the dominant surface air moisture source. Our methodology here is based on the use of the distillation model of *Johnsen et al.* [1989] tuned with the new supersaturation function (based on the NEEM δD - $\delta^{18}O$ slope) and the moisture source coherent with NEEM d-excess seasonal cycle as presented above. We base the use of this simple model on its ability to correctly simulate the isotopic variability of the precipitation samples. The model produces atmospheric vapor (at condensation height) above NEEM with high δD - $\delta^{18}O$ slope (8.1). This modeled condensating-vapor slope is very different from the slope of the collected surface vapor samples, (6.89 ± 0.15) (section 2.3). It is therefore unlikely that the majority of the sampled surface vapor is the “condensating” moisture at the origin of NEEM precipitation.

[35] We now explore the possible contribution of surface snow sublimation as a source for the collected vapor above the surface. The isotopic value of the condensate that is in isotopic equilibrium with the collected water vapor can be calculated using the in situ data available for surface temperature (T_s) by:

$$\delta_{\text{condensate}}^* = \alpha(T_s) \times \left(1 + \delta_{\text{vapor}}^*\right) - 1. \quad (3)$$

Here $\alpha(T)$ is the equilibrium fractionation coefficient over water or ice [*Majoube*, 1970; *Majoube*, 1971]. δ^* refers to either δD or $\delta^{18}O$. We consider both fractionation over ice and liquid, as several authors have reported a mesoscopic-liquid layer or quasi-liquid layer on the free surface of ice crystals down to -70°C [*Grannas et al.*, 2007; *Lied et al.*, 1994; *Wei et al.*, 2001]. Moreover, satellites using passive microwaves have detected episodic daily surface melt around NEEM (section 2.1).

[36] Using the water vapor data (shown with black crosses in Figure 4) the calculated isotopic composition of the condensate in isotopic equilibrium with the vapor have a δD - $\delta^{18}O$ slope of 7.64 ± 0.19 (for fractionation over ice, shown with filled diamonds in Figure 4) and 7.37 ± 0.17 (for fractionation over water, shown with open diamonds in Figure 4). This is comparable with the δD - $\delta^{18}O$ slope of the precipitation samples constituting the snow surface (7.57 ± 0.14 – shown with red circles in Figure 4). It is therefore very likely that the majority of the vapor above the snow surface is in isotopic equilibrium with the snow surface, with a combination of ice and liquid equilibrium fractionation. Figure 8 summarizes the observed information together with the Rayleigh model constraints on the δD - $\delta^{18}O$ slopes for precipitation, condensation moisture, or moisture formed at equilibrium with summer surface snow.

[37] We now discuss if the source of surface water vapor is the surface snow or older/deeper firn layers. Figure 3 shows a relationship between the isotopic composition of the latest precipitation and the isotopic composition of the water vapor. Between precipitation events, changes in the

isotopic composition of the sampled water vapor are observed. For group 1 of the water vapor samples, during the period no precipitation occurred, the change in δD is up to about 40‰ (Figure 3). These changes are larger than what can be explained by time varying temperature-dependent equilibrium fractionation effects starting from the same surface snow isotopic composition. This can be seen since the fractionation constant for δD only changes from ~ 1.12 at -5°C to ~ 1.15 at -20°C resulting in an approximate change in the δD of only about 15%. Our study of the δD - $\delta^{18}\text{O}$ slope rules out the hypothesis that the surface vapor consists of moisture from advection along the atmospheric paths delivering precipitation. One suggestion is that these changes in the isotopic composition of the sampled water vapor between two snowfall events could be explained by vapor originating from different depths below the snow surface. From Figure 2 the mean annual amplitude in δD of the snow is about 50‰. If the vapor would originate from the last winter snow layer, which in the summer time is to be found just 30–50 cm below the snow surface, a similar change in the isotopic value of the water vapor would be seen. Another suggestion is that these changes in the isotopic composition could be caused by different strengths of the katabatic winds bringing moisture down from upslope. None of these suggestions are possible to validate with the data set at hand but will be studied in the future.

[38] A further constrain on the processes driving variations of surface water vapor isotopic composition could be expected from its relationships with SH. Figure 4 clearly shows that different water vapor $\delta^{18}\text{O}$ – SH linear relationships are identified for the different observation periods. From the observed linear correlations obtained from water vapor monitoring conducted at Palisades, New York, *White and Gedzelman* [1984] attributed the changing correlation to the vertical gradients of both isotope composition and SH in the atmosphere. These vertical gradients are caused by air ascending under saturated conditions and becoming isotopically depleted because of condensation of the vapor. Changes in atmospheric vertical mixing are then expected to induce shifts in isotope values and SH. At NEEM, changes in vertical mixing linked with the boundary layer dynamics could explain the strong links between SH and isotopic composition of the water vapor above the snow surface, but cannot be reconciled with the observed δD - $\delta^{18}\text{O}$ slope. Neither could the observed relationship between δD and SH be explained by a Rayleigh distillation. If this was the case the logarithm to δD should be linear with the logarithm to SH when assuming a fixed source, which is not something we observe in the data. Alternatively, temporal changes in firm/low-atmosphere water vapor fluxes may also explain changing correlations between SH and $\delta^{18}\text{O}$, if different firm layers (with different $\delta^{18}\text{O}$ signatures) act as moisture sources for the lower atmosphere.

[39] It should be noted that we also find a similar high correlation between temperature and isotopic composition. We attribute the correlation between the isotopic value and temperature to be caused by correlation between SH and temperature. Because of the high correlation between isotopic composition and temperature or SH we will expect to see a diurnal cycle in the isotopic composition of the water vapor if the source is the snow surface. However, because of

the low temporal resolution we are not able to clarify this further with this data set.

5. Climatic Controls

5.1. Regression Analysis Between the NEEM Record and Climate Indices

[40] We first explore the linear correlations between regional climate indices and the NEEM shallow core back-diffused isotopes. A link would be expected from air mass trajectories (see section 4) between seasonal surface air temperatures at Ilulissat and Thule and interannual variations of NEEM seasonal isotope values (Table 3). However, we find that the mean annual temperatures at Ilulissat and Thule explain close to 0% of the variance in the mean annual isotope record. Instead when using the mean summer temperatures for JJA at Ilulissat (1965–2004) we find that they explain all of 21% of the variance in the mean annual isotope record (for the mean winter temperature DJF 4% of the variance is explained). However, it is interesting to note that when comparing temperatures for JJA at Ilulissat with summer isotope values at NEEM only 6% of the variance is explained (for the DJF temperature at Ilulissat compared with NEEM winter isotopes 0% variance is explained.)

[41] By contrast, the Baffin Bay Annual Sea Ice Anomaly (BBASIA) shows a strong correlation with the annual isotope signal at NEEM (34% variance explained). Both records display a strong anomaly for the years 1983–1984. However, they also have common variance for the rest of the overlapping time periods (Table 3). For Antarctica, coastal ice cores [*Masson-Delmotte et al.*, 2003] and modeling studies [*Noone and Simmonds*, 2004] have suggested similar links between the polar precipitation isotopic composition and variations in sea ice extent through changes in atmospheric condensation, evaporation, and mixing history. The strong correlation between NEEM isotope data and Baffin Bay sea ice extent is consistent with 3 day backward air trajectories calculated from the NEEM site (not presented here). The backward air trajectories showed that the majority of the air arriving to NEEM has traveled above the Baffin Bay area. In the work of *Fisher* [1990], the author reports that the coastal precipitation on Devon Island consisted of 18%–25% local moisture from the Baffin Bay, while on the top of Devon Island Ice Cap only 8% of the moisture would originate from the Baffin Bay. We have in this study not assessed the ratio of local moisture precipitating at NEEM. However, it could be speculated that it is not the direct coupling of local moisture precipitating at NEEM that results in the high correlation but merely a climatic connection between sea ice extent and the temperature in clouds and thereby the isotopic composition of the moisture. The interannual correlation reveals the potential of NEEM ice core isotopic data as an indicator of past sea ice extent in the Baffin Bay region.

[42] While NEEM isotopic records are weakly correlated with coastal Greenland mean annual temperatures, it must be noted that BBASIA and coastal temperatures at Thule and Ilulissat are themselves correlated (with R^2 of 0.37 and 0.56, respectively). We have also explored the correlations between our Greenland/Baffin Bay climate and isotopic records with North Atlantic indices. The North Atlantic Winter Sea Surface Temperature Anomaly (NAWSSTA,

Table 3. Correlation Between Global and Local Climate Variables, the Isotopic Record From NEEM07S3, and the Modeled REMOiso and LMDZiso Record

	Total Sea Ice Annual Anomaly	Baffin Bay Sea Ice Annual Anomaly	NAO Winter Anomaly	Ilulissat Annual Temp	Thule Annual Temp	NATL Annual	NATL Winter Anomaly	AO Winter Anomaly
Total sea ice annual anomaly	1979–2004 +0.04							
Baffin Bay sea ice annual anomaly	1979–2004 +0.10	1979–2004 +0.09						
NAO winter anomaly		1979–2004 -0.37	1951–2004 -0.08					
Ilulissat annual temp	1979–1999 0.00	1979–1999 -0.19	1961–1999 -0.19	1961–1999 + 0.03	1961–1999 + 0.16			
Thule annual temp	1979–2004 0.00	1979–2004 -0.27	1951–2004 -0.04	1951–2004 + 0.12	1961–1999 + 0.21			
NATL annual	1979–2004 -0.02	1979–2004 -0.15	1951–2004 -0.10	1951–2004 + 0.13	1961–1999 -0.27	1951–2004 + 0.60	1951–2004 -0.16	
NATL winter anomaly	1979–2004 + 0.12	1979–2004 + 0.16	1951–2004 + 0.53	1951–2004 -0.15	1961–1999 + 0.03	1951–2004 -0.08	1951–2004 -0.02	1965–2004 + 0.02
AO winter anomaly	1979–2004 0.00	1979–2004 -0.34	1965–2004 + 0.02	1965–2004 -0.00	1965–1999 -0.04	1965–2004 0.00	1965–2004 0.00	1965–2004 + 0.19
d-excess annual	1979–2004 -0.01	1979–2004 -0.01	1965–2004 + 0.11	1965–2004 -0.00	1965–1999 + 0.01	1965–2004 + 0.02	1965–2004 + 0.01	1965–2004 + 0.01
$\delta^{18}\text{O}$ winter value	1979–2004 -0.01	1979–2004 -0.18	1965–2004 -0.01	1965–2004 + 0.01	1965–1999 + 0.11	1965–2004 + 0.01	1965–2004 0.00	1965–2004 0.00
d-excess winter value	1979–2000 + 0.14	1979–2004 -0.24	1965–2004 -0.06	1965–2004 + 0.06	1965–1999 + 0.11	1965–2004 + 0.01	1965–2004 0.00	1965–2004 0.00
REMOiso $\delta^{18}\text{O}$ annual	1979–2000 -0.30	1979–2000 0.00	1959–2000 -0.21	1959–2000 -0.02	1961–1999 0.00	1959–2000 -0.01	1959–2000 0.00	1959–2000 -0.18
REMOiso d-excess annual	1979–2007 -0.05	1979–2007 -0.38	1979–2007 0.00	1979–2007 + 0.04	1979–1999 + 0.02	1979–2007 + 0.06	1979–2007 + 0.03	1979–2007 + 0.01
LMDZiso $\delta^{18}\text{O}$ annual	1979–2007 0.00	1979–2007 + 0.11	1979–2007 -0.01	1979–2007 0.00	1979–1999 + 0.02	1979–2007 0.00	1979–2007 0.00	1979–2007 0.00

^aIndicated is the variance explained (R^2) between two given records as well as the overlapping time period and whether it is a positive or negative correlation.

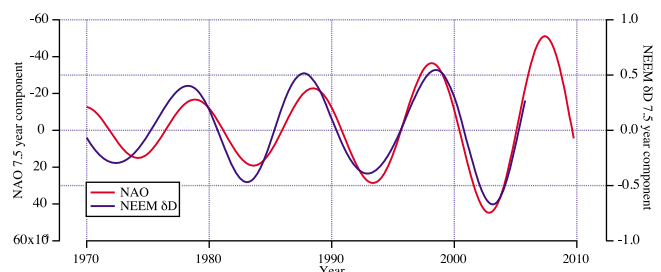


Figure 9. The 7.5 year bandpass-filtered δD signal compared to the 7.5 year bandpass-filtered NAO signal. Before 1970, effects due to edges are persistent and are not shown here.

measured for the region 5–20°N and 30–60°W) shows a link with BBASIA ($R^2 = 0.15$) but no link with the NEEM data (Table 3). Changes in winter air mass trajectories to Greenland are also known to be affected by changes in atmospheric dynamics in relationship with the North Atlantic Oscillation (NAO) [Sodemann *et al.*, 2008]. Previous studies have demonstrated the strong impact of the NAO on winter isotopic records from south and central Greenland ice core [Vinther *et al.*, 2003, 2010; White *et al.*, 1997]. As coastal temperature records from Ilulissat or Thule and Baffin Bay sea ice data record a NAO fingerprint in northwest Greenland, we expected to find a strong winter NAO signal in the NEEM shallow ice core isotopic records (Table 3). Surprisingly, neither annual nor winter NEEM $\delta^{18}\text{O}$ values from the NEEM07S3 core exhibit any significant relationship with NAO. In order to characterize the amplitude of isotopic variations expressed at the NAO time scale, we follow a previous methodology [White *et al.*, 1997] and use a bandpass filter to isolate the 7.5 year component of the δD record from the NEEM07S3 core (Figure 9). At NEEM, there is only 0.5‰ δD amplitude expressed in the 7.5 year component, which is at the limit of analytical noise and 8 times weaker than the 4‰ GISP2 δD amplitude, which was shown to be in phase with the NAO index for the last couple of decades. For NEEM, the winter NAO and AO index however accounts for ~11% and ~19%, respectively, of the variance in the annual d-excess signal, a feature expected from the imprint of NAO on NEEM source area SST and RH [Sodemann *et al.*, 2008].

[43] Using a multiple linear combination of the BBASIA with both the mean annual temperature at Ilulissat, the NAO winter index, and the NAWSSSTA, it is possible to explain up to 58% of the variance of NEEM07S3 interannual $\delta^{18}\text{O}$ variations (Table 4) (also without considering the 1983–84 anomaly). Despite the high correlation between Ilulissat summer temperature and the NEEM07S3 annual isotope record exchanging the Ilulissat annual temperature with summer temperature does not increase the variance explained by the above linear combination. Figure 7e shows the measured mean annual $\delta^{18}\text{O}$ record from the NEEM07S3 core compared to the estimation based on the multivariable linear regression explained above. Alternatively, a multiple linear combination of NEEM $\delta^{18}\text{O}$ and climate records can be proposed to quantify past variations in Baffin Bay sea ice, prior to the satellite era (1979). Figure 7h displays our Baffin Bay sea ice anomaly reconstruction. For the overlapping period the reconstruction represent 74% of the observed

Table 4. Variance of Isotope Record From NEEM07S3 Explained by a Multivariable Linear Regression of Baffin Bay Annual Sea Ice Anomaly, Ilulissat Annual Temperature, NAO Winter Anomaly, and the North Atlantic SST Winter Anomaly

	Baffin Bay Annual Sea Ice Anomaly	Baffin Bay ASIA + Ilulissat Annual Temp	Baffin Bay ASIA + NAO Winter Anomaly	Baffin Bay ASIA + Ilulissat Annual Temp + NAO Winter Anomaly	Baffin Bay ASIA + NAO Winter Anomaly + NATL Winter Anomaly	Baffin Bay ASIA + Ilulissat Annual Temp + NAO Winter Anomaly + NATL Winter Anomaly	Annual $\delta^{18}\text{O}$ + Ilulissat Annual Temp + NAO Winter Anomaly + NATL Winter Anomaly
Annual $\delta^{18}\text{O}$	$\alpha_1 = -0.58$ 33.7%	$\alpha_1 = -0.78,$ $\alpha_2 = -0.33$ 40.7%	$\alpha_1 = -0.69,$ $\alpha_2 = 0.35$ 44.8%	$\alpha_1 = -0.88,$ $\alpha_2 = -0.33,$ $\alpha_3 = 0.35$ 51.6%	$\alpha_1 = -0.79,$ $\alpha_2 = 0.29,$ $\alpha_3 = -0.32$ 53.5%	$\alpha_1 = -0.94,$ $\alpha_2 = -0.27,$ $\alpha_3 = 0.29,$ $\alpha_4 = -0.28$ 58.1%	
d-excess winter	$\alpha_1 = -0.48$ 23.9%	$\alpha_1 = -0.42,$ $\alpha_2 = 0.11$ 24.6%	$\alpha_1 = -1.14,$ $\alpha_3 = 0.49$ 29.2%	$\alpha_1 = -0.49,$ $\alpha_2 = 0.11,$ $\alpha_3 = 0.24$ 30.0%	$\alpha_1 = -0.58,$ $\alpha_3 = 0.23,$ $\alpha_4 = -0.05$ 29.4%	$\alpha_1 = -0.51,$ $\alpha_2 = 0.12,$ $\alpha_3 = 0.23,$ $\alpha_4 = -0.07$ 30.3%	
Baffin Bay annual sea ice anomaly							$\alpha_1 = -0.58,$ $\alpha_2 = -0.39,$ $\alpha_3 = 0.24,$ $\alpha_4 = -0.24$ 74.3%

^aThe coefficient estimates are given by α . All records have been normalized. Bold font indicates variance explained. Time period used is 1979–2004.

BBASIA variation. The reconstruction shows that prior to around 1995 the BBASIA is relatively flat besides the anomaly in 72/73, which were also found by *Mysak et al.* [1990], and the anomaly in 83/84. The 83/84 anomaly is also indicated by a low Cl⁻ concentration in the Penny Ice Cap core drilled in 1995 [*Goto-Azuma et al.*, 2002]. They also support the finding that the BBASIA is relatively flat before 1995. This indicates that the decrease in BBASIA have only been occurring over the last 15 years.

5.2. Correlation Analysis Between the NEEM Core and ERA-40

[44] We present here results from a correlation analysis of the ERA-40 data set [*Uppala et al.*, 2005] with the NEEM07S3 record. Significant ($p < 0.05$) correlation of the mean annual $\delta^{18}\text{O}$ signal and d-excess signal, with the mean annual 2 m temperature and wind speed at the 200 hPa level (the jet stream), respectively, is shown in Figure 10. In Figure 10a is seen a positive correlation between the $\delta^{18}\text{O}$ value and the temperatures in Baffin Bay and the Inuitian Region. Noticeable in Figure 10b is the significant positive correlation between $\delta^{18}\text{O}$ and the jet wind speed centered over 40°N 50°W. High cyclonic activity is often found below a strong jet stream (e.g., ch. 10.6 [*Holton*, 2004]). High cyclonic activity of this area increases the poleward flux of moisture, causing higher temperatures along the trajectory of the cyclonic systems. A significant positive correlation between strength of the jet stream above 40°N 50°W and the 2 m temperature over the ocean between Iceland and Greenland, and over the Baffin Bay, supports this (figure not shown). The area of positive correlation seen in the northern Pacific is related to a positive correlation between strength of jet stream for this area and 2 m temperature for the area of positive correlation seen in the

Atlantic Ocean between 25°N–40°N in Figure 10a. The correlation between strength of the jet stream over 40°N 50°W and the NEEM $\delta^{18}\text{O}$ signal indicate that the area around 40°N 50°W can be considered source region for the moisture ending up over the Baffin Bay and possibly over NEEM. This hypothesis is tested in Figure 10c, which shows the significant ($p < 0.05$) correlation between the 2 m temperature and the mean annual d-excess signal at NEEM. In this panel a region of positive correlation is seen in the eastern part of the Atlantic Ocean between 30° and 40°N. In section 4.1 this area was assumed to be a major source region for the moisture ending up at NEEM. This assumption is supported by the positive correlation, which is expected from the effect of kinetic fractionation during evaporation [*Merlivat and Jouzel*, 1979]. A similar significant correlation is found for the mean of the months May–June–July (minimum d-excess signal) but not for the months of November–December–January (maximum d-excess signal). We attribute this lack of significant correlation to the low winter precipitation amount. The “dipole”-like signal seen in the correlation between the NEEM d-excess signal and the strength of the jet stream (Figure 10d) over Iceland and the Azores, respectively, are correlated with the Arctic Oscillation (AO). This causes the wind speed over Iceland and the Azores to be correlated with the 2 m temperature in the Baffin Bay region and south of Greenland. Lower temperatures in the sink area result in more depletion of the isotopic signal in the precipitation, and therefore higher d-excess. This seems to indicate that the Baffin Bay and the ocean south of Greenland do not act as efficient source regions since a lower source temperature would result in lower d-excess [*Merlivat and Jouzel*, 1979]. The “dipole” structure of correlation seen in the middle of the Pacific is correlated with the temperature of the in section 4.1 assumed

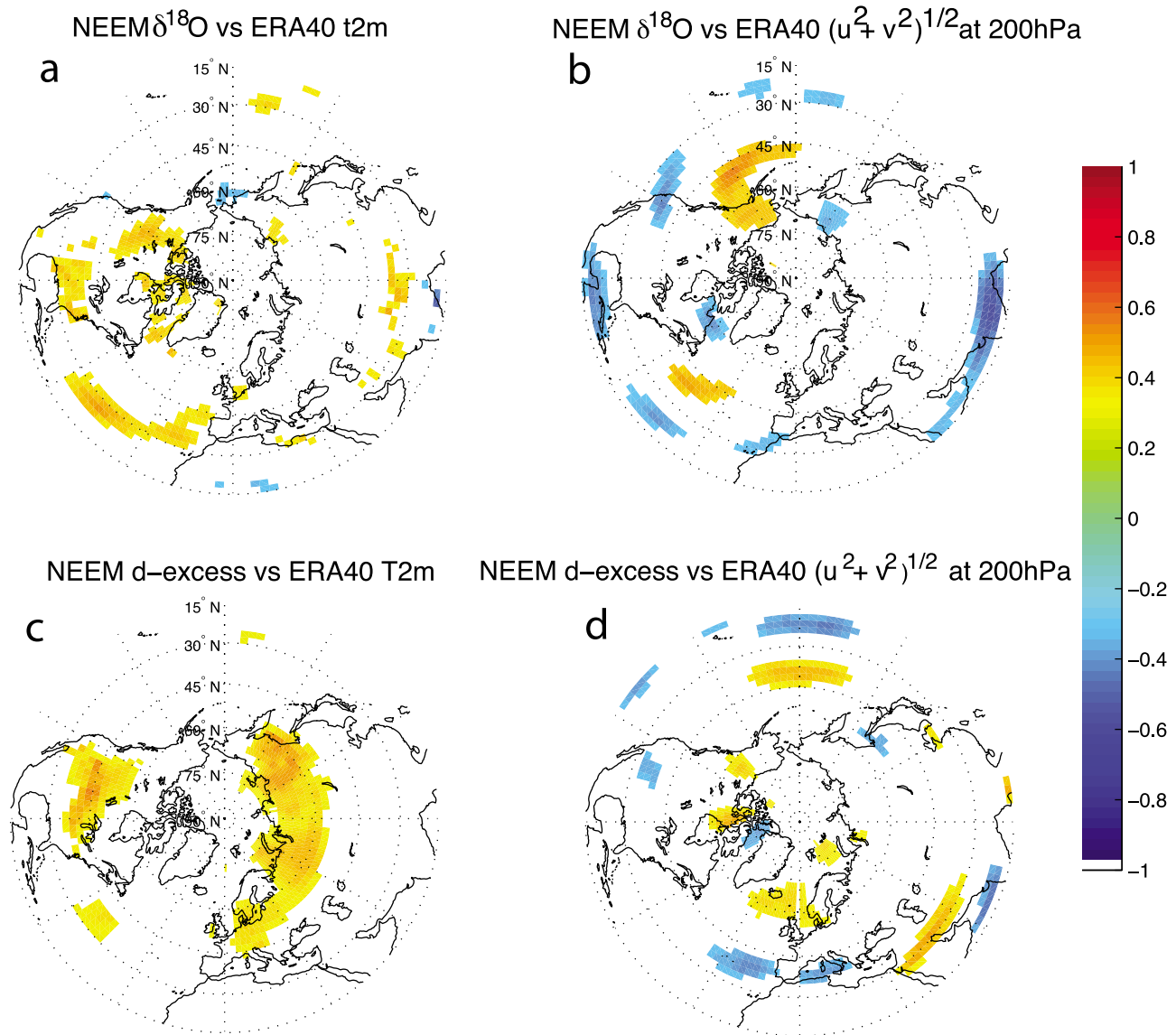


Figure 10. (a) The significant ($p < 0.05$, two-tailed) correlation between the mean annual NEEM $\delta^{18}\text{O}$ signal and the 2 m temperatures from ERA-40. (b) The significant ($p < 0.05$, two-tailed) correlation between the mean annual NEEM $\delta^{18}\text{O}$ signal and the ERA-40 wind speed at the 200 hPa level. (c) The significant ($p < 0.05$, one-tailed) correlation between the mean annual NEEM d-excess signal and the ERA-40 2 m temperatures. (d) The significant ($p < 0.05$, two-tailed) correlation between the mean annual NEEM d-excess signal and the ERA-40 wind speed at the 200 hPa level.

source region, thereby controlling the d-excess of the initial vapor through the kinetic effects [Merlivat and Jouzel, 1979].

6. Regional to General Circulation Model Outputs for NEEM

6.1. Seasonality of Precipitation

[45] The winter NAO signal is only very weakly represented in the NEEM isotope record compared to winter ice core isotopic records from other sites on the Greenland ice sheet [Vinther et al., 2003; White et al., 1995] and winter coastal meteorological data. One explanation for the lack

of a clear NAO signal might be a lack of winter precipitation at the NEEM site, as indicated by satellite data from CALIPSO (presented in section 2.1). Due to the lack of year-round precipitation data, we rely on atmospheric models. In Figure 11 is shown the ratio between precipitation for JJA and DJF as estimated from two regional atmospheric models (MAR and REMO) [Fettweis, 2007; Sturm et al., 2005], one stretched grid atmospheric general circulation model (LMDZ) [Krinner et al., 1997], and two coupled ocean-atmosphere models (IPSL VERSION, CNRM-IPCC, and CNRM-new). Apart from the CNRM-new model, all the other models indicate between 2.5 and 4.5 times more accumulation during the summer than the

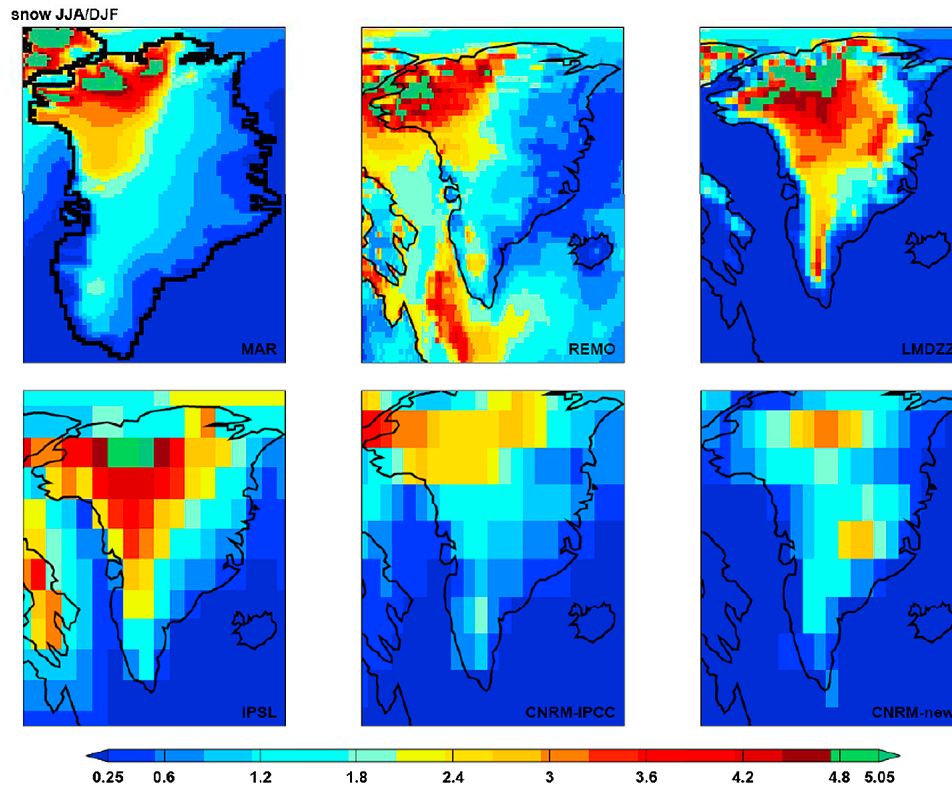


Figure 11. The mean summer (JJA) to winter (DJF) ratio in amount of precipitation over 20 years of simulation (1980–1999). Estimates are from the MAR model, REMOiso, LMDZ, IPSL, CNRM-IPCC, and CNRM-new.

winter period in a large part of the northwest Greenland including the NEEM site. The lack of winter versus summer precipitation is also observed on the neighboring Penny Ice Cap where summer accumulation were 4 times larger than winter accumulation [Goto-Azuma *et al.*, 2002]. This supports our hypothesis that the weak NAO imprint on NEEM data is linked with intermittency of winter precipitation and will have implications for the interpretation of the deep ice core data. However, it seems that coupled climate models still preserve this feature, which means that paleoclimate simulations may resolve such seasonality features [Krinner and Werner, 2003].

6.2. Interannual Isotopic Variability at NEEM

[46] Two isotopic simulations are explored here, one conducted with a general circulation model (LMDZiso) and one conducted with a regional atmospheric model (REMOiso). The water isotope-enabled general atmospheric circulation LMDZiso [Risi *et al.*, 2010a] has been run nudged (Newtonian relaxed toward the observed field [von Storch *et al.*, 2000]) to the ERA-40 analyses for the time period 1979–2002 and to ECMWF operational analysis for the time period 2003–2007. The model has a warm winter bias in temperature and simulates about 54 cm of water precipitation per year (two times the estimated NEEM accumulation). As a result, it has a systematic bias on NEEM $\delta^{18}\text{O}$, with the simulated values at least 5‰ above the mean NEEM2007S1 data. It simulates too low a d-excess, with a seasonal cycle in perfect antiphase with the site temperature

and $\delta^{18}\text{O}$ (Figure 12). At the interannual scale, LMDZiso simulates a strong (4‰ in annual mean) $\delta^{18}\text{O}$ depletion in 1983–84 (Figure 13). The $\delta^{18}\text{O}$ –temperature temporal slope simulated at the interannual scale is around 0.6‰/K for NEEM. A small inverse correlation is simulated between LMDZ DJF NAO and NEEM $\delta^{18}\text{O}$ ($R \sim -0.4$).

[47] An independent 42 year simulation (1959–2000) is available from the regional REMOiso model [Sturm *et al.*, 2005] nudged by the ERA-40 reanalyses (J. Sjolte *et al.*, Modeling the water isotopes in Greenland precipitation 1959–2001 with the meso-scale model REMOiso, submitted to *Journal of Geophysical Research*, 2011). The REMOiso has a spatial resolution of $\sim 2.8^\circ \times 2.8^\circ$ (approximately 55 km in Greenland) and 19 vertical levels. LMDZ-iso: 2.5° in latitude \times 3.75° in longitude with 19 vertical levels. As for LMDZiso, the REMOiso systematically underestimates Greenland isotopic depletion by 10‰ (Figure 12) associated with a similar temperature bias. The simulated $\delta^{18}\text{O}$ seasonal cycle amplitude is twice as large as observed. Albeit each seasonal cycle appears shifted when compared to the data, the phase lag between the modeled d-excess cycle and modeled $\delta^{18}\text{O}$ cycle is comparable with the phase lag between the observed d-excess cycle and the observed $\delta^{18}\text{O}$ cycle (Figure 12). The mean annual $\delta^{18}\text{O}$ and d-excess is shown in Figure 13. It is seen that the REMOiso simulation shows a similar decrease in $\delta^{18}\text{O}$ for the 1983–84 event as the LMDZiso simulation. However, none of the models are able to recreate the magnitude of the observed 1983–84 event depletion. The same is observed for the d-excess. In

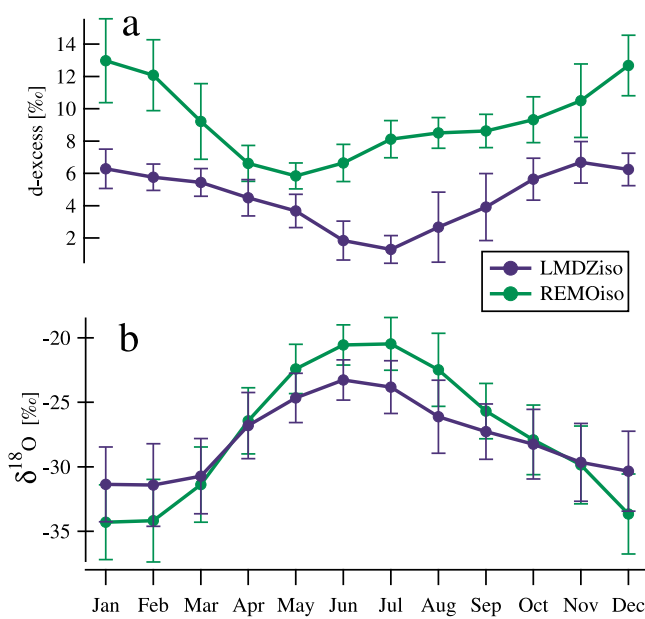


Figure 12. The annual cycle in $\delta^{18}\text{O}$ and d-excess for both the REMOiso and LMDZiso simulation of the isotopic content of the precipitation at NEEM.

general there is a higher correlation in between the models compared to the correlation between the models and the observed isotopic record of the NEEM07S3 core.

[48] From the REMOiso 42 year simulation, a synthetic ice core record can be produced (accounting for precipitation seasonality and isotopic diffusion) and compared to the observations. The result shows weak correlation with the NEEM07S3 core annual isotopic signal ($R^2 = 0.11$ for $\delta^{18}\text{O}$ and 0.07 for d-excess). Comparing a 28 year (1979–2007) simulation using LMDZiso reveal a strong correlation with the NEEM07S3 core annual $\delta^{18}\text{O}$ isotopic signal ($R^2 = 0.49$ for $\delta^{18}\text{O}$ and 0.07 for d-excess). It is therefore of interest to understand what controls the isotopic value in the modeled REMOiso and LMDZiso record in comparison with our analysis of correlations with regional climate indices. (Table 3). Noticeably when only correlating the NEEM07S3 core annual $\delta^{18}\text{O}$ with the REMOiso and LMDZiso for the overlapping period from 1979 to 2000 they both show a correlation of about $R^2 = \sim 0.32$. However, irrespectively of the time period (1965–2000 or 1979–2000) the simulated REMOiso $\delta^{18}\text{O}$ at the NEEM site has no correlation with BBASIA. This can suggest that despite using the ERA-40 synoptic wind data, REMOiso does not capture the correct moisture transport trajectories linked with cyclonic activity over the Baffin Bay area. However, as seen in Table 3 LMDZiso $\delta^{18}\text{O}$ correlates strongly with BBASIA, which probably explains the high correlation between the modeled and observed annual isotope signal at NEEM. Comparably does the Total Sea Ice Annual Anomaly correlate with REMOiso $\delta^{18}\text{O}$ with a correlation of $R^2 = 0.14$ while it does not correlate with LMDZiso over the same period. It should be noted that the correlations between LMDZiso $\delta^{18}\text{O}$ and the different climate indices shown in Table 3 are approximately the same

as the correlation between the NEEM07S3 $\delta^{18}\text{O}$ annual record and the same climate indices. This suggests that the LMDZiso better captures the large-scale drivers of inter-annual variability at NEEM. A detailed comparison between LMDZiso and REMOiso would likely reveal what physics is important in simulating the right isotopic composition of the precipitation in Greenland. It seems that the difference between the two models is either in the forcing of SST and sea ice cover or in the parameterized physics.

[49] A comparison of the correlation between the REMOiso modeled annual $\delta^{18}\text{O}$ record and the LMDZiso modeled record for the period 1979–2000 reveals a high correlation coefficient of $R^2 = 0.45$. If performing a multivariable linear correlation of the BBASIA and the REMOiso modeled annual $\delta^{18}\text{O}$ against the LMDZiso modeled annual $\delta^{18}\text{O}$ a high correlation of $R^2 = 0.57$ is observed. This suggests that the observed signal at NEEM is a sum of a large-scale signal captured by the models and a local signal not captured by especially REMOiso.

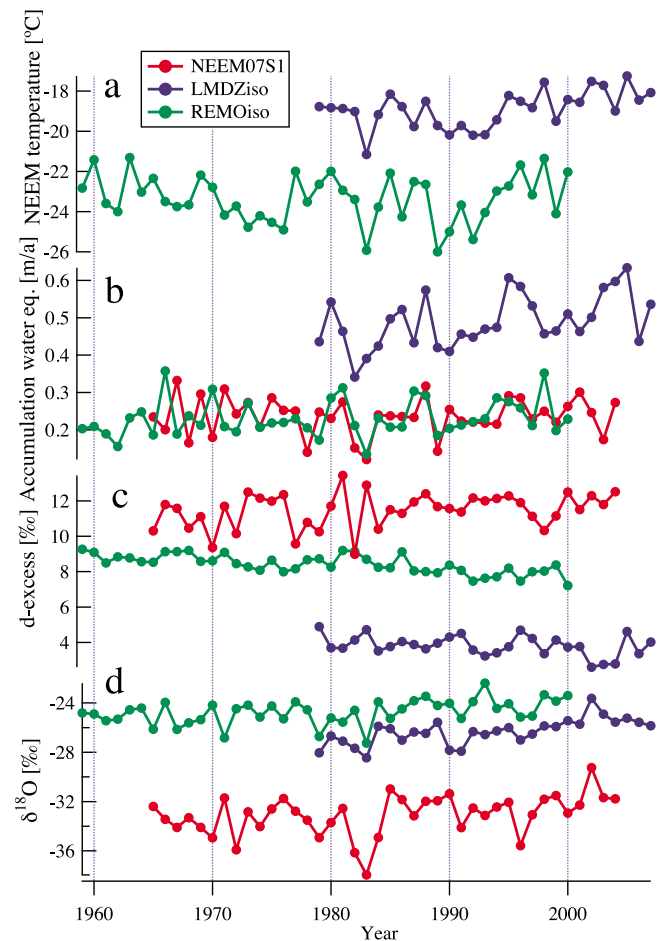


Figure 13. Comparison of the interannual variability of the REMOiso and LMDZiso model output compared to the observed values from the NEEM07S3 core. (a) The simulated mean annual site temperature at NEEM for the nearest grid point in the model. (b) The modeled and observed mean accumulation rate in meter per year water equivalent. (c) and (d) The d-excess and $\delta^{18}\text{O}$, respectively, from the REMOiso and LMDZ models and the NEEM07S3 core.

[50] Over the period 1979–2000, the REMOiso model simulates a NEEM $\delta^{18}\text{O}$ increasing trend with a magnitude of $\sim 2.1\text{‰}$ (to compare with $\sim 2.2\text{‰}$ observed for the period 1979–2000). The LMDZiso simulates for the period 1979–2000 an increase of $\sim 1.5\text{‰}$ in $\delta^{18}\text{O}$ at NEEM. By contrast, both the REMOiso and LMDZiso model simulates a d-excess decreasing trend of 1.2‰ (1979–2000) and 0.3‰ (1979–2000), respectively, opposite to the observed 0.4‰ increasing trend (1979–2000). Following the work of Jouzel *et al.* [2007] and Masson-Delmotte *et al.* [2005] this leads to an interpretation using the REMOiso and LMDZiso model of a cooling of the source region while the NEEM07S3 records points to a warming of the source region. Using the relationship between site and source temperature and change in $\delta^{18}\text{O}$ and d-excess value derived by Masson-Delmotte *et al.* [2005] by use of the distillation MCIM model developed by Ciais and Jouzel [1994] gives a change according to the REMOiso model of about $+1.5^\circ\text{C}$ and -1.3°C for the site and source temperature over the period 1979–2000. For the LMDZiso model the numbers are $+1.7^\circ\text{C}$ and 0.0° , respectively. For the NEEM07S3 record the numbers are $+3.3^\circ\text{C}$ and $+1.3^\circ\text{C}$, respectively. This calculated warming of the site region follows the previous reported warming (section 3.1) using the empirical relationship between mean annual isotope value and temperature reported by [Johnsen *et al.*, 1999] ($\sim 3.0 \pm 1.2^\circ\text{C}$ for the last ~ 40 years).

7. Conclusion

[51] Combining the data from shallow cores, precipitation and water vapor samples with the meteorological observations at NEEM have revealed information on the external factors affecting the NEEM snow isotopic composition as well as indicating a strong link between the surface water vapor isotopic composition and the surface snow.

[52] From the precipitation samples, which were collected during the season of 2008, we observe changes of up to 90‰ in the δD content of the precipitation samples during the passage of a cyclonic system. This is relatively large compared to the annual amplitude of 50‰ in δD . By adjusting the supersaturation function of a Rayleigh model, we are able to capture the observed δD - $\delta^{18}\text{O}$ slope in the precipitation samples. With the new supersaturation we are able to simulate the annual d-excess cycle, which, after back-diffusion correction, shows a 5 months lag with respect to $\delta^{18}\text{O}$. Our simple modeling approach is compatible with a NEEM moisture source region as far south as SHIP E (35°N , 48°W).

[53] Using a simple isotope distillation model, we also show that the water vapor collected above the snow surface has a very small, if any, fingerprint of the vapor in the clouds bringing in precipitation to the NEEM site. Comparing the relationship between δD and $\delta^{18}\text{O}$ of the collected water vapor with the precipitation samples points to the water vapor being in isotopic equilibrium with the surface snow. This has implications for our understanding of the post depositional processes affecting the connection between the climate and the isotopic composition observed in the ice core. The water vapor samples also show varying relationships with specific humidity, which we are not able to explain using the data at hand. The relationship between humidity and isotope composition should also results in a

diurnal cycle. However, we do not have enough temporal resolution to observe this. By monitoring the snowpack temperature and the air temperature it should be possible to determine whether the correlation between humidity and isotope values is because of variations in the snowpack or variations in the boundary layer. Our observations suggest that diurnal variations should be resolved in atmospheric water vapor composition, a feature which will be assessed by deploying new types of water vapor laser analyzers at NEEM to perform high temporal resolution monitoring.

[54] When studying the isotopic composition of the shallow cores, it is interesting to note the very low correlation between the NAO index and the annual/winter isotope records. This is likely caused by more frequent accumulation during summer than during winter. Such a seasonal bias will most likely be more pronounced during the glacial period, which will have to be considered for the use of isotopes as a palaeothermometer and possibly for the identification of seasonal cycles and dating. Our data reveal an imprint of changes in Baffin Bay area sea ice extent in the interannual variability of NEEM isotope records. This opens up for the possibility of estimating the Baffin Bay sea ice extent prior the onset of satellite observations in 1979. Over the last 40 years, significant trends in the NEEM isotope record reveals a warming trend of NEEM temperature as well as its mean moisture source. Our estimate of NEEM warming ($\sim 3.0^\circ\text{C}$ over the last 40 years) will have to be compared to borehole temperature data and will have implications for the use of firn air data. Preliminary comparisons between NEEM isotopic data and isotopic results obtained from regional and general circulation atmospheric models have revealed model biases regarding the present-day seasonal cycle and the drivers of interannual variability. However, models seem to capture the observed increasing trend. This will have implications for the use of climate/atmospheric models when interpreting the deeper part of the NEEM ice core. Performing water-tagging simulations with general circulation models together with detailed trajectory analysis are likely to reveal more detailed information about the relationship between climate and the isotopes found at NEEM.

Appendix A

A1. Precipitation Collection Procedure

[55] The sampling of precipitation at NEEM was carried out by setting up a table made out of wood with a surface area of 0.35 m^2 in the clean-air zone upwind of camp. The table was equipped with 15 cm high sides to prevent snow from blowing off the table. To reduce the collection of wind-drifted snow, the height of the table was about 1.6 m above the snow surface. Regardless of wind speed we never registered any snow on the table during nonprecipitation days. The inside of the table was painted white to reduce the amount of absorbed sunlight. During precipitation events snow was collected about every 3 h depending on the amount of snow caught on the table. The samples were kept frozen until both $\delta^{18}\text{O}$ and δD were measured at the Centre for Ice and Climate using a Thermo Finigan Delta Vplus mass spectrometer with an accuracy ($\pm 1\sigma$) of 0.08‰ and 0.5‰ for $\delta^{18}\text{O}$ and δD , respectively (Figure 3).

A2. Procedure for Atmospheric Water Vapor Collection

[56] The air intake was placed 3 m above the snow surface and air was pumped through the vapor trap with a flow rate of about 5 L per minute. The temperature of the vapor trap was kept at -80°C and by filling the trap with glass beads of a diameter of 2 mm the surface area was increased to ensure complete condensation of all the vapor. After 2 h sampling, 2 to 3 ml of water were collected depending on the humidity in the atmosphere. The sampled water vapor was transferred into vials, which were kept frozen, until $\delta^{18}\text{O}$ and δD mass spectrometer measurements were performed at the Centre for Ice and Climate. The transfer of the water vapor was achieved by connecting a vial and the vapor trap and hereafter creating a vacuum of 10^{-2} mbar. By heating the vapor trap but keeping the vial at -80°C the vapor was transferred to the vial by sublimation from the beads in the vapor trap and then condensation in the vial. Laboratory experiments with this setup and standard water samples have shown that the sample transfer leads to uncertainties in $\delta^{18}\text{O}$ and δD values of $\pm 0.2\text{‰}$ and $\pm 1\text{‰}$, respectively, and that no detectable water vapor is able to get through the vapor trap at the flow rate used.

[57] **Acknowledgments.** NEEM is directed and organized by the Center of Ice and Climate at the Niels Bohr Institute and U.S. NSF, Office of Polar Programs. It is supported by funding agencies and institutions in Belgium (FNRS-CFB and FWO), Canada (GSC), China (CAS), Denmark (FIST), France (IPEV and INSU/CNRS), Germany (AWI), Iceland (Rannls), Japan (NIPR), Korea (KOPRI), the Netherlands (NWO/ALW), Sweden (VR), Switzerland (SNF), United Kingdom (NERC) and the United States (U.S. NSF, Office of Polar Programs). ECMWF ERA-40 data used in this study have been obtained from the ECMWF data server. The authors gratefully acknowledge the NOAA Air Resources Laboratory (ARL) for the provision of the HYSPLIT transport and dispersion model and/or READY Web site (<http://www.arl.noaa.gov/ready.html>) used in this publication. The authors thank Christophe Sturm for access to REMOiso model output.

References

- Abdalati, W., and K. Steffen (2001), Greenland ice sheet melt extent: 1979–1999, *J. Geophys. Res.*, *106*, 33,983–33,988, doi:10.1029/2001JD900181.
- Armengaud, A., et al. (1998), Deuterium excess in Greenland snow: Analysis with simple and complex models, *J. Geophys. Res.*, *103*(D8), 8947–8953, doi:10.1029/98JD00274.
- Barlow, L. K., et al. (1993), The North Atlantic oscillation signature in deuterium and deuterium excess signals in the Greenland Ice Sheet Project 2 ice core, 1840–1970, *Geophys. Res. Lett.*, *20*(24), 2901–2904, doi:10.1029/93GL03305.
- Ciais, P., and J. Jouzel (1994), Deuterium and oxygen 18 in precipitation: An isotopic model including mixed cloud processes, *J. Geophys. Res.*, *99*(D8), 16,793–16,804, doi:10.1029/94JD00412.
- Craig, H., and L. I. Gordon (1965), Deuterium and oxygen 18 variations in the ocean and the marine atmosphere, in *Stable Isotopes in Oceanographic Studies and Paleotemperatures, July 26–30 1965, Spoleto, Italy*, edited by E. Tongiorgi, pp. 9–130, Cons. Naz. delle Ric. Lab. di Geol. Nucl., Pisa, Italy.
- Dansgaard, W. (1964), Stable isotopes in precipitation, *Tellus*, *16*(4), 436–468, doi:10.1111/j.2153-3490.1964.tb00181.x.
- Dansgaard, W. (1969), Oxygen-18 analysis of water, *Medd. Groenl.*, *177*(2), 33–36.
- Dansgaard, W., et al. (1982), A new Greenland deep ice core, *Science*, *218*(4579), 1273–1277, doi:10.1126/science.218.4579.1273.
- Dansgaard, W., et al. (1993), Evidence for general instability of past climate from a 250-kyr ice-core record, *Nature*, *364*(6434), 218–220, doi:10.1038/364218a0.
- Draxler, R. R., and G. D. Rolph (2003), HYSPLIT (Hybrid Single-Particle Lagrangian Integrated Trajectory) Model access via NOAA ARL READY Web site (<http://www.arl.noaa.gov/HYSPLIT.php>), NOAA Air Resour. Lab., Silver Spring, Md.
- Fettweis, X. (2007), Reconstruction of the 1979–2006 Greenland ice sheet surface mass balance using the regional climate model MAR, *Cryosphere*, *1*(1), 21–40, doi:10.5194/tc-1-21-2007.
- Fisher, D. A. (1990), A zonally averaged stable-isotope model coupled to a regional variable-elevation stable-isotope model, *Ann. Glaciol.*, *14*, 65–71.
- Fisher, D. A. (1991), Remarks on the deuterium excess in precipitation in cold regions, *Tellus, Ser. B*, *43*(5), 401–407, doi:10.1034/j.1600-0889.1991.t01-4-00006.x.
- Fisher, D. A., and B. T. Alt (1985), A global oxygen isotope model semi-empirical zonally averaged, *Ann. Glaciol.*, *7*, 117–124.
- Fisher, D. A., et al. (1985), Stratigraphic noise in time series derived from ice cores, *Ann. Glaciol.*, *7*, 76–83.
- Goto-Azuma, K., et al. (2002), An ice-core record over the last two centuries from Penny Ice Cap, Baffin Island, Canada, *Ann. Glaciol.*, *35*(1), 29–35, doi:10.3189/172756402781817284.
- Grannas, A. M., et al. (2007), An overview of snow photochemistry: Evidence, mechanisms and impacts, *Atmos. Chem. Phys.*, *7*(16), 4329–4373, doi:10.5194/acp-7-4329-2007.
- Grotes, P. M., and M. Stuiver (1997), Oxygen 18/16 variability in Greenland snow and ice with 10^{-3} - to 10^5 -year time resolution, *J. Geophys. Res.*, *102*(C12), 26,455–26,470, doi:10.1029/97JC00880.
- Hammer, C. U. (1980), Acidity of polar ice cores in relation to absolute dating, past volcanism, and radio-echoes, *J. Glaciol.*, *25*(93), 359–372.
- Herron, M. M., and C. C. Langway Jr. (1980), Firm densification: An empirical model, *J. Glaciol.*, *25*(93), 373–385.
- Hoffmann, G., et al. (1998), Water isotope module of the ECHAM atmospheric general circulation model: A study on timescales from days to several years, *J. Geophys. Res.*, *103*(D14), 16,871–16,896, doi:10.1029/98JD00423.
- Holton, J. R. (2004), *An Introduction to Dynamic Meteorology*, Elsevier Acad. Press, Burlington, Mass.
- IAEA/WMO (1969–1979), Environmental isotope data No. 1–6. World survey of isotope concentration in precipitation, *Tech. Rep. Ser.*, *96*, *117*, *129*, *147*, *165*, *192*, IAEA, Vienna.
- Johnsen, S. J. (1977), Stable isotope profiles compared with temperature profiles in firn and with historical temperature records, in *Proceedings of Symposium on Isotopes and Impurities in Snow and Ice, I.U.G.G. XVI, General Assembly, Grenoble Aug. Sept., 1975, Int. Assoc. of Hydrol. Sci. Publ. 118*, pp. 388–392, Int. Assoc. of Hydrol. Sci., Washington, D. C.
- Johnsen, S. J., et al. (1989), The origin of Arctic precipitation under present and glacial conditions, *Tellus, Ser. B*, *41*(4), 452–468, doi:10.1111/j.1600-0889.1989.tb00321.x.
- Johnsen, S. J., et al. (1999), Stable isotope records from Greenland Deep Ice Cores: The climate signal and the role of diffusion, in *Ice Physics and the Natural Environment*, edited by J. S. Wettlaufer et al., pp. 89–107, Springer, Berlin.
- Johnsen, S. J., et al. (2000), Diffusion of stable isotopes in polar firn and ice: The isotope effect in firn diffusion, in *Physics of Ice Core Records*, edited by T. Hondoh, pp. 121–140, Hokkaido Univ. Press, Sapporo, Japan.
- Jouzel, J., and L. Merlivat (1984), Deuterium and oxygen 18 in precipitation: Modeling of the isotopic effects during snow formation, *J. Geophys. Res.*, *89*(D7), 11,749–11,757, doi:10.1029/JD089iD07p11749.
- Jouzel, J., et al. (2007), The GRIP deuterium-excess record, *Quat. Sci. Rev.*, *26*(1–2), 1–17, doi:10.1016/j.quascirev.2006.07.015.
- Krinner, G., and M. Werner (2003), Impact of precipitation seasonality changes on isotopic signals in polar ice cores: A multi-model analysis, *Earth Planet. Sci. Lett.*, *216*(4), 525–538, doi:10.1016/S0012-821X(03)00550-8.
- Krinner, G., et al. (1997), Studies of the Antarctic climate with a stretched-grid general circulation model, *J. Geophys. Res.*, *102*(D12), 13,731–13,745, doi:10.1029/96JD03356.
- Lee, J.-E., I. Fung, D. J. DePaolo, and C. C. Henning (2007), Analysis of the global distribution of water isotopes using the NCAR atmospheric general circulation model, *J. Geophys. Res.*, *112*, D16306, doi:10.1029/2006JD007657.
- Lied, A., et al. (1994), Glancing angle X-ray scattering from single-crystal ice surfaces, *Phys. B*, *198*(1–3), 92–96.
- Majoube, M. (1970), Fractionation factor of ^{18}O between water vapour and ice, *Nature*, *226*(5252), 1242, doi:10.1038/2261242a0.
- Majoube, M. (1971), Fractionnement en oxygène 18 et en deutérium entre l'eau et sa vapeur, *J. Clim. Phys.*, *68*, 1423–1436.
- Masson-Delmotte, V., et al. (2003), Recent southern Indian Ocean climate variability inferred from a Law Dome ice core: New insights for the interpretation of coastal Antarctic isotopic records, *Clim. Dyn.*, *21*(2), 153–166, doi:10.1007/s00382-003-0321-9.

- Masson-Delmotte, V., et al. (2005), Holocene climatic changes in Greenland: Different deuterium excess signals at Greenland Ice Core Project (GRIP) and NorthGRIP, *J. Geophys. Res.*, *110*, D14102, doi:10.1029/2004JD005575.
- Masson-Delmotte, V., et al. (2006), Past and future polar amplification of climate change: Climate model intercomparisons and ice-core constraints, *Clim. Dyn.*, *26*(5), 513–529, doi:10.1007/s00382-005-0081-9.
- Masson-Delmotte, V., et al. (2008), A review of Antarctic surface snow isotopic composition: Observations, atmospheric circulation, and isotopic modeling, *J. Clim.*, *21*(13), 3359–3387, doi:10.1175/2007JCLI2139.1.
- Mathieu, R., D. Pollard, J. E. Cole, J. W. C. White, R. S. Webb, and S. L. Thompson (2002), Simulation of stable water isotope variations by the GENESIS GCM for modern conditions, *J. Geophys. Res.*, *107*(D4), 4037, doi:10.1029/2001JD900255.
- Merlivat, L., and J. Jouzel (1979), Global climatic interpretation of the deuterium-oxygen 18 relationship for precipitation, *J. Geophys. Res.*, *84*(C8), 5029–5033, doi:10.1029/JC084iC08p05029.
- Mysak, L. A., et al. (1990), Sea-ice anomalies observed in the Greenland and Labrador Seas during 1901–1984 and their relation to an interdecadal Arctic climate cycle, *Clim. Dyn.*, *5*, 111–133, doi:10.1007/BF00207426.
- Noone, D., and I. Simmonds (2002), Associations between delta O-18 of water and climate parameters in a simulation of atmospheric circulation for 1979–95, *J. Clim.*, *15*(22), 3150–3169, doi:10.1175/1520-0442(2002)015<3150:ABOOWA>2.0.CO;2.
- Noone, D., and I. Simmonds (2004), Sea ice control of water isotope transport to Antarctica and implications for ice core interpretation, *J. Geophys. Res.*, *109*, D07105, doi:10.1029/2003JD004228.
- North Greenland Ice Core Project Members (2004), High resolution climate record of the Northern Hemisphere reaching into the last Glacial Interglacial Period, *Nature*, *431*(7005), 147–151, doi:10.1038/nature02805.
- Petit, J. R., et al. (1991), Deuterium excess in recent Antarctic snow, *J. Geophys. Res.*, *96*(D3), 5113–5122, doi:10.1029/90JD02232.
- Picard, G., et al. (2007), Surface melting derived from microwave radiometers: A climatic indicator in Antarctica, *Ann. Glaciol.*, *46*(1), 29–34, doi:10.3189/172756407782871684.
- Risi, C., S. Bony, F. Vimeux, and J. Jouzel (2010a), Water-stable isotopes in the LMDZ4 general circulation model: Model evaluation for present-day and past climates and applications to climatic interpretations of tropical isotopic records, *J. Geophys. Res.*, *115*, D12118, doi:10.1029/2009JD013255.
- Risi, C., A. Landais, S. Bony, J. Jouzel, V. Masson-Delmotte, and F. Vimeux (2010b), Understanding the ¹⁷O excess glacial-interglacial variations in Vostok precipitation, *J. Geophys. Res.*, *115*, D10112, doi:10.1029/2008JD011535.
- Schmidt, G. A., G. Hoffmann, D. T. Shindell, and Y. Hu (2005), Modeling atmospheric stable water isotopes and the potential for constraining cloud processes and stratosphere-troposphere water exchange, *J. Geophys. Res.*, *110*, D21314, doi:10.1029/2005JD005790.
- Sodemann, H., V. Masson-Delmotte, C. Schwierz, B. M. Vinther, and H. Wernli (2008), Interannual variability of Greenland winter precipitation sources: 2. Effects of North Atlantic Oscillation variability on stable isotopes in precipitation, *J. Geophys. Res.*, *113*, D12111, doi:10.1029/2007JD009416.
- Steffen, K., and J. Box (2001), Surface climatology of the Greenland ice sheet: Greenland Climate Network 1995–1999, *J. Geophys. Res.*, *106*(D24), 33,951–33,964, doi:10.1029/2001JD900161.
- Steffen, K., et al. (1996), Greenland Climate Network: GC-Net, *CRREL 96–27 Special Report on Glaciers, Ice Sheets and Volcanoes, Tribute to M. Meier, CRREL Spec. Rep. 96–27*, edited by S. C. Colbeck, pp. 98–103, CRREL, Hanover, N. H.
- Sturm, K., et al. (2005), Simulation of delta O-18 in precipitation by the regional circulation model REMOiso, *Hydrol. Process.*, *19*(17), 3425–3444, doi:10.1002/hyp.5979.
- Tindall, J. C., P. J. Valdes, and L. C. Sime (2009), Stable water isotopes in HadCM3: Isotopic signature of El Niño–Southern Oscillation and the tropical amount effect, *J. Geophys. Res.*, *114*, D04111, doi:10.1029/2008JD010825.
- Torinesi, O., et al. (2003), Variability and trends of the summer melt period of Antarctic ice margins since 1980 from microwave sensors, *J. Clim.*, *16*(7), 1047–1060, doi:10.1175/1520-0442(2003)016<1047:VATOTS>2.0.CO;2.
- Trigo, I. F. (2006), Climatology and interannual variability of storm-tracks in the Euro-Atlantic sector: A comparison between ERA-40 and NCEP/NCAR reanalyses, *Clim. Dyn.*, *26*(2–3), 127–143, doi:10.1007/s00382-005-0065-9.
- Uppala, S. M., et al. (2005), The ERA-40 re-analysis, *Q. J. R. Meteorol. Soc.*, *131*(612), 2961–3012, doi:10.1256/qj.04.176.
- Vaughan, M. A., et al. (2009), Fully automated detection of cloud and aerosol layers in the CALIPSO lidar measurements, *J. Atmos. Oceanic Technol.*, *26*(10), 2034–2050, doi:10.1175/2009JTECHA1228.1.
- Vinther, B. M., S. J. Johnsen, K. K. Andersen, H. B. Clausen, and A. W. Hansen (2003), NAO signal recorded in the stable isotopes of Greenland ice cores, *Geophys. Res. Lett.*, *30*(7), 1387, doi:10.1029/2002GL016193.
- Vinther, B. M., et al. (2009), Holocene thinning of the Greenland ice sheet, *Nature*, *461*(7262), 385–388, doi:10.1038/nature08355.
- Vinther, B. M., et al. (2010), Climatic signals in multiple highly resolved stable isotope records from Greenland, *Quat. Sci. Rev.*, *29*(3–4), 522–538, doi:10.1016/j.quascirev.2009.11.002.
- von Storch, H., et al. (2000), A spectral nudging technique for dynamical downscaling purposes, *Mon. Weather Rev.*, *128*(10), 3664–3673, doi:10.1175/1520-0493(2000)128<3664:ASNTFD>2.0.CO;2.
- Wei, X., et al. (2001), Surface vibrational spectroscopic study of surface melting of ice, *Phys. Rev. Lett.*, *86*(8), 1554–1557, doi:10.1103/PhysRevLett.86.1554.
- Wen, X.-F., S.-C. Zhang, X.-M. Sun, G.-R. Yu, and X. Lee (2010), Water vapor and precipitation isotope ratios in Beijing, China, *J. Geophys. Res.*, *115*, D01103, doi:10.1029/2009JD012408.
- Werner, M., et al. (2001), Isotopic composition and origin of polar precipitation in present and glacial climate simulations, *Tellus, Ser. B*, *53*(1), 53–71, doi:10.1034/j.1600-0889.2001.01154.x.
- White, J. W., and S. D. Gedzelman (1984), The isotopic composition of atmospheric water vapor and the concurrent meteorological conditions, *J. Geophys. Res.*, *89*(D3), 4937–4939, doi:10.1029/JD089iD03p04937.
- White, J. W. C., et al. (1995), Deuterium excess and δD in the GISP2 ice core: Reconstructions of ocean conditions from ice cores, paper presented at GISP/GRIP Symposium, Wolfboro, N. Y., September.
- White, J. W. C., et al. (1997), The climate signal in the stable isotopes from Summit, Greenland: Results of comparisons with modern climate observations, *J. Geophys. Res.*, *102*(C12), 26,425–26,439, doi:10.1029/97JC00162.

F.-M. Bréon, S. Falourd, J. Jouzel, M. Kageyama, V. Masson-Delmotte, B. Minster, and H. J. Punge, Laboratoire des Sciences du Climat et de l'Environnement/IPSL, CEA-CNRS-UVSQ, CE Saclay, F-91191 Gif/Yvette, France.

H. B. Clausen, D. Dahl-Jensen, S. J. Johnsen, H. Løcherer, J. Sjolte, H. C. Steen-Larsen, A. Svensson, and B. M. Vinther, Centre for Ice and Climate, Niels Bohr Institute, University of Copenhagen, Juliane Maries Vej 30, DK-2100 Copenhagen, Denmark. (hanschr@gfy.ku.dk)

X. Fettweis, Inst Climatol, Univ Liege, B-4000 Liege, Belgium.

H. Gallée and G. Picard, Laboratoire de Glaciologie et Géophysique de l'Environnement, Saint Martin d'Hères CEDEX, F-38402, France.

C. Risi and K. Steffen, Cooperative Institute for Research in Environmental Science, University of Colorado, Campus Box 216, Boulder, CO 80309, USA.

D. Salas, CNRM/GMGEC, Météo-France, CNRS, F-31057 Toulouse CEDEX, France.

J. Schwander, Physics Institute, Climate and Environmental Physics, University of Bern, CH-3012 Bern, Switzerland.

A. E. Sveinbjörnsdóttir, Science Institute, University of Reykjavik, Dunhaga 3, Reykjavik 107, Iceland.

J. White, Institute of Arctic and Alpine Research, University of Colorado, Campus Box 450, Boulder, CO 80309, USA.